CERN/SPSC/78-130
SPSC/P119

24 October 1978

PROPOSAL TO THE SPSC

PROPOSAL TO SEARCH FOR NEW PARTICLES

CERN[1]-LAPP[2]-MIT[3]-NIKHEFF[4] COLLABORATION

U. Becker[1], J. Bron[4], D. Buikman[4], J. Burger[3],
M. Chen[3], P. Duinker[4], M. Hodous[3], M. Fujisaki[3],
T. Matsuda[3], D. Novikoff[3], S. Sugimoto[3] and F. Vannucci[2]

This proposal was written during the year 1978 by

Samuel C.C. Ting and his colleagues

from CERN, LAPP, MIT, NIKHEFF, Niels Bohr Inst., Univ. of Helsinki, and others. The full participation list will be submitted later.

ABSTRACT

We intend to continue our search for new particles at the newly built $\bar{p}p$ collider by detecting their single μ, μ-pair, or multimuon decays. The pair mass resolution is $\Delta m/m \simeq 1\%$ at $m \simeq 100$ GeV. The detector, a solenoidal magnet with projection drift chambers, and a hadron absorber placed immediately around the beam pipe, is a third generation detector built by us to search for new particles.

1. INTRODUCTION

Since the discovery of the J particle at Brookhaven National Laboratory, many groups have been engaged in the continuing study of lepton pairs at higher masses at higher energy accelerators.

The idea of C. Rubbia, P. McIntyre and D. Cline[1] has stimulated great progress towards achieving a high-energy $\bar{p}p$ collision ring of 270 × 270 GeV at the CERN Super Proton Synchrotron (SPS) [2]. We propose a detector to use this facility to search for new particles.

In recent years we have built two $\sim 4\pi$ detectors to study muon pairs.

1.1 At the ISR

At the CERN Intersecting Storage Rings (ISR) we have designed detector[3]. to study muon pairs, which can stand a luminosity of 10^{32} cm^{-2} sec^{-1} and reach down to a sensitivity of 10^{-37} cm^2 after one year of running. The detector covers a mass region from the mass of the J to the kinematic limit of 60 GeV. It has the following characteristics which ensured the success of the experiment.

i) The detector is made out of $\sim$ 600 tons of magnetized iron excited to a field of 18 kG, sandwiched with 800 m^2 of drift chambers and 200 m^2 of trigger counters. The detector is shielded from the intersection region by at least 50 cm of iron (see Fig. 1). In the forward region the detector is further protected by a specially designed conical-shaped lead box which reduces the decay distances from π and K decays. This arrangement enables us to stop almost all the soft hadrons and to select and reconstruct events without contamination due to spurious tracks.

ii) By using electronic logic requiring two muons coming out from the intersection region at least 90° apart in ϕ, by using programmable branch drivers to ensure that at least six out of the (normally) eight drift chambers are fired, and by properly using the shielding and veto counters surrounding the beam pipes upsteam and downstream, we have been able to reduce the trigger rate from 10^4/sec to 0.5/sec at a luminosity of 10^{31} cm^{-2} sec^{-1} at a centre-of-mass energy of 62 GeV, while 10^7 charged particles are produced every second. From the analysis of our data, we have found that most of the backgrounds are not correlated but are random hits from muons along the beam pipe and from low-energy particles floating around the intersection region. A fast microprocessor is, therefore, the ideal means of reducing this type of background.

Figures 2a and 2b show a schematic view of an event detected in the apparatus. In Fig. 2a 14 tracks are seen in the inner detector built inside the magnetized iron, while, as shown in Fig. 2b, only two tracks, corresponding to the muons, succeed in traversing the first absorber.

Figure 3 shows the resulting plot of dimuon masses obtained with an integrated luminosity of 2.6×10^{37} cm^{-2}, corresponding to about 3 months of data taking. Events with high mass are essentially produced back to back and detected mainly near 90°.

In the mass region $4 < m < 8$ GeV the cross-section falls off 2 orders of magnitude. In the mass region of 8 to 11 GeV the data are dominated by the production of upsilons. The observed structure is in reasonable agreement with the expected resolution of the detector, which is $\Delta m/m \leq 10\%$ (σ). There have been many theoretical and experimental studies of muon pair production. The solid curve in Fig. 3 is a zero parameter prediction based on a scaling model [the so-called Drell-Yan[4] mechanism] used by Kinoshita, Satz and Schildknecht[5] (KSS), who have analysed the Fermilab data and have found them to be in agreement with an analytical form

$$m^3 \left.\frac{d\sigma}{dmdy}\right|_{y=0} = C_{DY} \left\{1 - \frac{m}{\sqrt{s}}\right\}^{10}$$

with $C_{DY} = 1.3 \times 10^{-5}$ mb GeV^2.

The agreement between our data and the (KSS) prediction is truly amazing since our measured cross-section is between a factor of 30 (at 4 GeV mass) to 200 (at 12 GeV mass) higher than the lower-energy data measured at Fermilab[6]. To have the data in agreement with the predictions of the Drell-Yan mechanism over such a large range is the strongest experimental evidence supporting the Drell-Yan model.

There are strong indications of events at mass 20 $\sim$ 30 GeV which are being analysed. These events would clearly indicate that very unusual phenomena are occurring. The limitation of such a detector is visible in Fig. 3 at the place of the T signal. Because of multiple scattering in the iron, the resolution $\Delta m/m$ is of the order of 10%; it improves only slowly with the iron thickness. Therefore, it is impractical to try to achieve substantially better mass resolution by increasing the iron thickness. To reach 1% mass resolution and to select clean muon events, it is therefore necessary to separate the functions of momenta determination and hadron filtering.

1.2 At PETRA

At PETRA we are building a second-generation detector[7] to continue our search for new particles up to 30 GeV mass with a high mass resolution of 20 MeV (determined by the quantum fluctuation of PETRA), and to measure down to a 1% level the interference effects between weak and electromagnetic interactions. This detector, shown in Fig. 4a,b, covers muon pairs down to 10°, and muon tracks are measured by drift chambers and magnetized iron yokes. Hadrons are measured by calorimeters. The construction of the detector is very similar to that of the ISR detector, with the drift chambers well protected from the intersection region. Great care is taken in the design and survey of the chambers to ensure that the systematic bias is less than 1%. To ensure that we can measure muon-pair asymmetry down to 1%, the detector can rotate 180° in ϕ angle and 180° in θ to cancel out any detector bias.

To trigger the drift chambers, a pattern recognition device[8] was designed which enables us, in 50 nsec, to sort out all combinations from various scintillation counters, lead-scintillator counters, and lucite counters. The device also allows us to make a quicker measurement of the pulse height of the combination so as to reduce the trigger rate.

2. PHYSICS MOTIVATION

The purpose of the present experiment is to continue our study of lepton pair production in hadron-hadron collisions up to the highest possible energy and up to the highest possible pair mass. We list the following examples of items of particular interest to us:

i) to search for more families of unexpected particles above PETRA energy;

ii) to search for the neutral vector boson $Z^0 \to \mu^-\mu^+$; its yield is 3-4 orders of magnitude above the Drell-Yan pairs, and its mass is estimated to be near 80-90 GeV region[9,10];

iii) to compare our results with e^+e^- pair experiments as an experimental verification of μe universality at $q^2 \approx 10^4$ GeV^2.

We note that observation of a peak in the $\mu^-\mu^+$ pair mass spectra near the 80-90 GeV region does not imply that a Z^0 has been found. To distinguish a Z^0 from a ρ, ω, ϕ, or a J-like particle, we have to observe three more properties of the new peak:

1) the width of the peak should be $\Gamma \approx \alpha m$, $\alpha^{-1} = 137$;

2) the observed cross-section should be several orders of magnitude above a J-like particle;

3) the decay $Z^0 \to \mu^-\mu^+$ should have a charge asymmetry[11].

To accomplish the above points implies that the detector must have a resolution of $\Delta m/m \simeq 1\%$ and that it must have a large solid angle and cover $\mu^-\mu^+$ pairs down to small forward-backward angles, thus enabling us to measure a possible asymmetry.

3. DESIGN CONSIDERATIONS

To continue our search for new particles to the highest possible mass, we propose a new muon pair detector at the $\bar{p}p$ colliding machine. Our design for the new detector is based on the following physics considerations and on experience.

3.1 Hadron rejection and triggering

We will keep the good features of the ISR detector, namely the cleanliness of the events and the low trigger rate. To this end, we propose to absorb most of the hadrons near the intersection point and detect only muons. We can improve on our present ISR detector by placing a thick tungsten-uranium absorber immediately surrounding the vacuum pipe. Instead of the $\sim$ 1 m free decay length that we had at ISR, we will now have 15 cm of decay length for hadrons.

3.2 To reject hadron punch-throughs, large-angle single scattering, etc.

We still identify muons by the absorber/drift chamber sandwich technique, and arrange our trigger counters and logic processor closely following the ISR and PETRA designs.

3.3 To improve mass resolution to $\sim$ 1%

We first measure the muon momentum and angle with a large-volume projection chamber in a strong magnetic field produced by an aircore solenoid magnet. Such a magnet gives a bending in the plane perpendicular to the beam axis. In this plane the vertex is a well-defined point, and this configuration is best adapted for obtaining good pattern recognition.

3.4 A 4π solid angle

In order to study the properties of new particles, such as forward-backward asymmetry, and in order to collect a large amount of events, the detector is symmetrical in both the θ and the ϕ directions and accepts muons down to $\theta = 20°$.

3.5 Familiar technology

We maintain a capacity to withstand high interaction rates using verified techniques. In our detector at the ISR we have

$$10^{31} \times 40 \times 10^{-27} = 4 \times 10^{5} \text{ interactions/sec} .$$

The sensivity time of our drift chambers is 2 μsec. The chance of having two interactions in the chambers is then $2 \times 10^{-6} \times 4 \times 10^{5} = 0.8$. With an average multiplicity of 20 particles/interaction, 16 particles accompany a muon pair during the sensitive time of the drift chambers. Experimentally, we observe an upper limit of 3% muon events accompanied by one track in a chamber placed after three absorption lengths of absorber. Therefore the observed rejection is 0.03/16 = 0.2%. At the $\bar{p}p$ machine we expect

$$10^{30} \times 60 \times 10^{-27} = 6 \times 10^{4} \text{ interactions/sec .}$$

This machine being bunched with a bunch spacing time of 3.8 μsec, the chance of two events occurring in the same chamber is $6 \times 10^{4} \times 3.8$ μsec = 0.25. This is smaller than at the ISR.

With an average multiplicity of 60, a dimuon pair will be accompanied by $60 \times 0.25 = 15$ particles coming from a second interaction. With an arrangement similar to the one of the ISR, the number of tracks associated with a μ pair will be approximately

$$15 \times 2 \times 10^{-3} = 3\% \ .$$

4. THE DETECTOR

The detector is shown in Figs. 5 and 6. It has the following elements.

4.1 The absorber

On the basis of our experiment at the ISR we propose to use a total of 30 cm of uranium and tungsten (5 collision lengths) and copper, positioned immediately around the vacuum pipe to absorb hadrons. A few collision lengths of degrader at a large angle are very effective in suppressing soft hadron background, as we have verified experimentally at the ISR. With $m_{\mu\mu} > 3$ GeV and $\sqrt{s} = 62$ GeV, we found that about < 3% of the dimuons have some associated particles penetrating 5 collision lengths or 50 cm of Fe.

The tungsten and uranium cylinder has a length of 60 cm, and the total weight is 4.5 tons. On the two sides there is a copper absorber of 90 cm length to reject small-angle hadrons. Both ends are easily accessible and there is enough space for a sturdy support. Outside the absorber is a layer of 48 triggering counters A, and two layers of proportional tubes with delay line read-out which measure the longitudinal position of tracks to an accuracy of 1 cm. An important point to notice is that, because high-mass events are essentially produced back to back, the uncertainty in the angle between the two tracks contributes negligibly to the mass resolution near the Z^0 mass. The momentum resolution dominates. As the momenta are measured outside of the absorber the multiple scattering does not spoil the mass resolution. Only the energy loss has any importance. This can easily be corrected, and the error due to straggling is very small.

4.2 The central drift chamber

We propose to use a projection drift chamber similar to the ones now being installed in the JADE-detector in PETRA [12,13], one cell of which is shown in Fig. 7, where high spatial resolution is achieved by high gas pressure and by multiple sampling of the track. These chambers will be contained in a 4 atm cylinder. From the result of the JADE experiment we know that with standard electronics this allows us to achieve a spatial resolution better than 150 μm. To limit the maximum drift space to about 10 cm, we will use 48 cells, each of them covering an angle of 7.5° in azimuth. In the middle plane, 120 signal wires spaced every 1 cm are put at ground voltage. High-voltage wires operated at 2.5 kV separate the signal wires and shape the electrical field. High-voltage strips on the wall of the cells give uniform electric field throughout the chamber.

The technical feasibility of the detector has been tested by the JADE experiment. Figure 8 shows the end section of a pressure vessel, developed for the JADE experiment, which is able to sustain 4 atm of gas and allows the easy change of a broken wire. The electronics are outside the vessel and attached to it.

4.3 The magnet

In order to achieve good momentum resolution together with compactness, we propose to use a solenoidal magnet with a magnetic field of 14 kG. The inner diameter of the coil will be 3.5 m and the length 4.5 m. It will thus be possible to measure tracks with polar angles as small as 20°. After allowing for the thickness of the absorber, etc., the maximum radial track projection for each muon is 1.2 m.

The flux return will be an iron cylinder which fits closely around the coil and which has disk-like end-caps which could be made from yokes 3 and 4 of experiment R209. The radial thickness of the cylinder has been chosen to be 60 cm and the thickness of the end-caps will be 70 cm. The external dimensions of the detector are 6 m × 6 m × 8 m. The field strength in the flux return can be limited to 16 kG. The total weight of the iron will be 580 tons.

The copper coil will have a radial thickness of 35 cm. Of this, the equivalent of 10 cm will be occupied by cooling water and insulation, and if the mean coil temperature can be held at 30°C, the power dissipation will be 4.8 MW. The total weight of copper will be 120 tons.

Feasibility studies[14] and the experience of experiments at PETRA, where similar magnets have been built, show that there is no problem in building such a magnet and that the construction should take less than one year.

4.4 Large drift chambers and counters outside the return yokes

Outside the return yokes the detector is surrounded by 48 triggering counters B in the central region and by 48 element triggering counters in the front and 48 element triggering counters in the back.

To further reject hadron punch-through and hadron showers, we place large drift chambers outside the return yokes in the same way as we did in the ISR and PETRA detector[15]. A total area of 220 m^2 outside the magnet yokes is covered by drift chambers. Each chamber has four planes measuring the exit position of the muon to 700 μm (r.m.s.). Planes corresponding to parallel signal wires from two outer chambers are separated by a minimum of 10 cm. The exit angle of muons is therefore measured to better than 7 mrad (r.m.s.). We intend to use the existing chambers from our ISR experiment R209 for this purpose. As seen in Figs. 5 and 6, these chambers fit perfectly for the present geometry. No other work is needed in operating these chambers and the corresponding 6000 wires of electronics.

5. DATA COLLECTION

5.1 The triggering system

Again the trigger logic and the pattern recognition device are similar to the ones used at the ISR and PETRA experiments. Figures 5, 6 and 9 show the counter arrangement. Two layers of counters will be used to trigger on dimuon events: 48 counters A positioned after the central absorber, 48 counters B after the return yoke to cover the barrel part, and 48 fan-shaped C counters for each end-cap. Figure 10 shows the schematic of the trigger logic. Each phototube is monitored by an ADC, a TDC, and a scaler, and each counter has one tube at each end. A mean-timer will be used for the two tubes to obtain better time resolution. All tube signals will be gated with the beam gate. Signals from B and C counters are logically added together sector by sector, and define the outside D sectors. In order to divide the azimuth into finer sections the counters will overlap as shown in Figs. 9 and 10, defining a total of 96 equal sectors. This represents effective widths for A and B counters of 7.3 cm and 36 cm, respectively. One candidate muon is defined by coincidence of one inside sector F_j and three outside sectors E_j, E_{j-1}, E_{j+1}. We call this trigger G_j. The trigger on high-mass dimuons is formed by the coincidence between G_j and G_{j+36}, to G_{j+50}; thus the two tracks have an angle between them larger than 90°. This will also allow us to have a mass cut between the two muon tracks which can be determined during the experiment.

To trigger on single muons we set up an additional logic requirement of a minimum p_T of 5 GeV/c at the level of the counters. The longitudinal coordinate will be measured by proportional tubes and outside drift chambers and checked by the TOF measurement of the two phototubes at the end of each counter. The mean-timer output from the end-cap counters C are summed together for each end and delayed with respect to each other for additional beam-gas and stray muon rejection.

In addition to beam gate, cosmic rays can also be rejected by the difference of flight time in the top and bottom B counters as shown in Fig. 10.

5.2 Trigger rate

For events satisfying the initial counter trigger, a more stringent requirement is applied on the drift chamber wires. This is done either with a microprocessor or with a hard-wired trigger box. More specifically for each muon candidate, we demand a total of at least 50 wires fired at the inner projection chamber and two or more space points formed in the outside muon chambers, in the same sector as the trigger counter sector. Based on our experience at the ISR, we estimate that the trigger rate for dimuons at the $\bar{p}p$ collider will be less than 0.1/sec. The trigger rate for single muons at the ISR is 70/sec with a luminosity of 10^{31} cm^{-2} sec^{-1}. At the $\bar{p}p$ collider, we expect the trigger rate to be scaled down by

$$(70/\text{sec}) \times \left(\frac{24}{96}\right) \times \frac{1}{10} = 2/\text{sec} ,$$

where the factor 24/96 is the ratio of combinations between the inner and the outer hodoscope at the ISR and $\bar{p}p$, and the factor or 1/10 is the ratio of luminosity. The trigger rate is dominated by random coincidences, since the expected genuine high p_T hadron ($p_T \gtrsim 5$ GeV) rate is about 0.5/sec before and 0.02/sec after the inner absorber.

6. ACCEPTANCE AND RESOLUTION

The drift chambers measure the muon trajectory in the angular range $20 < \theta < 160°$. Therefore the solid angle covered is approximately 94% of 4π. The momentum resolution in the projection chamber is[16]:

$$\frac{\delta p_T}{p_T} = \frac{3.3 \times 10^3}{B(\text{kG})L^2(\text{cm}^2)}\, p_T\, \delta x \sqrt{A} ,$$

where δx is 150 μm and where

$$A = \frac{720}{N + 5} .$$

N is the number of measurements on a given track. Here we have 120 signal wires and the resolution goes roughly as $1/\sqrt{N}$.

In our case we have

$$\frac{\delta p_T}{p_T} = \frac{3.3 \times 10^3}{14(125)^2} \, 150 \times 10^{-4} \sqrt{\frac{720}{125}} \, p_T$$

$$= 5.6 \times 10^{-4} \, p_T .$$

As example, the intermediate vector boson Z^0, if it has a mass of 80 GeV, will decay into two muons of average momentum 40 GeV:

$$p_T = 40 \sin\theta \qquad \text{GeV/c} .$$

In this case our detector will measure a

$$\frac{\delta p_T}{p_T} = 2.2\% \sin\theta$$

for $40° < \theta < 140°$.

With the outside drift chambers and the proportional tubes we can determine the polar angle for each track within 4 mrad. This is essential for measuring the p_L of each muon and also for energy loss correction in the central absorber.

The momentum resolution of each muon is

$$\left\langle \left(\frac{\delta p}{p}\right)^2 \right\rangle = \left\langle \left(\frac{\delta p_T}{p_T}\right)^2 \right\rangle + \left\langle \left(\frac{\delta\theta}{\tan\theta}\right)^2 \right\rangle$$

$$\approx \left\langle \left(\frac{\delta p_T}{p_T}\right)^2 \right\rangle .$$

The mass resolution of the muon pair is therefore

$$\left\langle \frac{\delta m}{m} \right\rangle = \frac{1}{\sqrt{2}} \sqrt{\left\langle \left(\frac{\delta p}{p}\right)^2 \right\rangle + \left\langle \left(\frac{\sin\theta_{\mu\mu} d\theta}{1 - \cos\theta_{\mu\mu}}\right)^2 \right\rangle}$$

$$\approx \frac{1}{\sqrt{2}} \sqrt{\left\langle \left(\frac{\delta p}{p}\right)^2 \right\rangle} \qquad \text{for } \theta_{\mu\mu} \sim 180° ,$$

where $\theta_{\mu\mu}$ is the opening angle between the two muons.

The dependence of $\delta m/m$ on the production angle θ is shown in Fig. 11a. As seen, one can achieve the mass resolution of 1.4% in most of the solid angle, and the resolution is adequate enough to determine the charge of the muons for the measurement of charge asymmetry in the range of

$$-0.94 < \cos\theta < 0.94 \ .$$

As a measure of the acceptance of the detector for μ pairs, we have assumed that a neutral vector boson is produced with an $X_f \approx 2p_L/\sqrt{s}$ distribution of

$$\frac{d\sigma}{dX_f} \propto (1 - X_f)^3$$

as expected in an annihilation mechanism. We have also made the pessimistic assumption that it is completely polarized and therefore decays with a $(1 + \cos^2\theta^*)$ distribution. In Fig. 11b the total acceptance and the "very high resolution" acceptance is shown as a function of mass. In the 80 GeV region the total acceptance is 92%, and the acceptance with r.m.s. mass resolution of 1.4% is 65%.

7. RATES

The Drell-Yan mechanism gives a good representation of the dimuon production at sufficiently high mass and energy. It predicts a scaling formula

$$m^3 \frac{d\sigma}{dm} = F(\tau) \ ,$$

where $F(\tau)$ is a universal function of the dimensionless variable $\tau = m/\sqrt{s}$. Our results at the ISR shows that scaling works well between Fermilab/SPS energies and ISR energies, and that the formula

$$m^3 \left.\frac{d\sigma}{dm dy}\right|_{y=0} = 1.3 \left(1 - \frac{m}{\sqrt{s}}\right)^{10} \times 10^{-32} \ \mathrm{cm}^2 \ \mathrm{GeV}^2$$

represents well the experimental data for $\sqrt{s}$ from 20 to 62 GeV. We use the same formula to predict the rate that we expect at the $\bar{p}p$ collider. We have to correct for the gain coming from the fact that $\bar{p}$ has valence antiquarks. The ratio of dimuon production in $\bar{p}p$ and pp is taken from Peierls[3)] et al. This gain as a function of the dimuon mass is plotted on Fig. 12 together with the resulting cross-section.

For Z^0 production[9-11)], the cross-section is 3 to 4 orders of magnitude higher than the continuum and is also shown in Fig. 12. The resulting numbers of events obtained in 300 hours of running time in our detector is 80. The luminosity has been taken equal to 10^{30} cm^{-2} s^{-1}, and the Z^0 mass is chosen in the range of 80-90 GeV. It is apparent that at the level of one event in 300 hours, there is nothing above 35 GeV mass except for the Z^0 peak. This also means that, should a new family of particles decaying into $\mu^+\mu^-$ exist, it could be seen in our detector with mass resolution of $\sim$ 1% and negligible background, provided it has a reasonable cross-section and small width.

For a search for charged W's by detecting $W^{\pm} \to \mu\nu$, the cross-section is expected to be higher than that for Z^0. Our detector would be able to see 300 $W^+ \to \mu^+$ and 300 $W^- \to \mu^-$ decays in 300 hours.

8. THE IMPORTANCE OF RESOLUTION

We have designed a detector with very good mass resolution ($\sim$ 1%) for the following reasons:

1) With a resolution of $\sim$ 1% the Z^0 peak will show up clearly in 1 or 2 bins with low background even if the $\bar{p}p$ luminosity is a factor of 10 below design value.

2) There is no reason to believe that there is only one neutral vector boson Z^0. If there is a series of Z^0's, a good mass resolution will facilitate their separation into several peaks, as opposed to a broad resonance which would be seen with poorer resolution.

3) One of the crucial elements of the Weinberg-Salam model is the existence of a Higgs scalar boson. Whereas the nature of this particle is not well known, it is likely that it can decay into a pair of J-like particles, which in turn decay to four μ's

$$p + \bar{p} \to H + X$$
$$\quad \hookrightarrow J + J$$
$$\qquad J \to \mu^+\mu^-$$
$$\qquad J \to \mu^+\mu^-$$

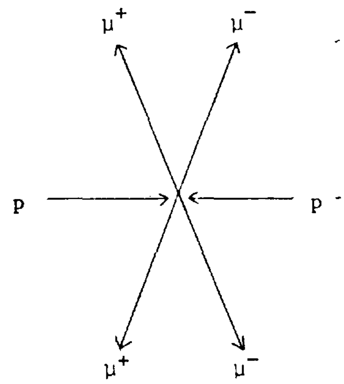

or it can decay into a pair of low-mass virtual Z^0's, which then decay to pairs of muons:

$p + \bar{p} \to H + X$

$\quad \hookrightarrow Z^0 + Z^0$

$\qquad\qquad\quad \hookrightarrow \mu^+\mu^-$

$\quad\quad \hookrightarrow \mu^+\mu^-$

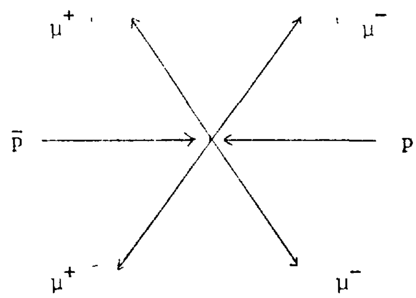

With our near 4π acceptance and good momentum resolution, we can measure the four muon tracks and reconstruct the Higgs boson mass. We have calculated the resolution for both decay modes and a Higgs mass of 60 GeV, and found that our mass resolution will be better than 1%.

9. BACKGROUNDS

9.1 Rejection of cosmic rays

One of the main backgrounds in a large-area detector comes from cosmic rays. At 60 m under ground, only very few cosmic rays traverse the inner hodoscope every second. The outer scintillators are 6 m apart. This means that the difference in timing between cosmic rays and particles coming from the vertex is, at minimum, 18 nsec. We have achieved 0.5 nsec accuracy in large scintillation counters by measuring the TOF at both ends at R209. Furthermore, with the machine being run in bunched mode, a 5 nsec beam gate will cut down cosmic-ray triggers by another factor or $\sim$ 1000. All these cuts bring the on-line cosmic-ray background to a completely negligible level. There are other off-line cuts against cosmic rays: collinearity, vertex reconstruction, and the fact that the momentum of the lower track is systematically 1.5 GeV lower than the upper track because of energy loss in the absorber.

9.2 Hadron punch-through

To evaluate hadron punch-through, we use the measured particle distribution[17)]

$$E\,\frac{d^3\sigma}{dp^3} = 10^{-30}\cdot\left[\frac{10^4}{p_T^{8.6}} + 1.3\,\frac{1}{p_T^4}\right]\,(1-x_T)^{9.76}\ .$$

We further make the most pessimistic assumption that high p_T hadrons are completely correlated; namely, a 40 GeV/c p_T hadron is accompanied with a second 40 GeV/c p_T hadron produced in the opposite hemisphere.

The calculation of hadron punch-through takes the following steps for each hadron:

i) passing through a minimum of 30 cm or 3 absorption lengths of tungsten + uranium;

ii) the energy loss in the absorber is about 700 MeV/c and particles with less than 800 MeV/c left after the absorber will be spiraling in the 14 kG magnet and will not hit the outside hodoscope. Therefore there is a natural cut of 1.5 GeV below which particles will not reach the hodoscope.

iii) for energetic hadrons, the copper coil and the iron yoke, which have a total of 5 absorption lengths, will cause surviving hadrons to deviate from their original trajectory, and thus, by placing drift chambers outside the iron yoke measuring the direction of outgoing hadrons to 7 mrad (r.m.s.), will reduce this background by a factor of approximately 80.

Taking all these things into account, Fig. 13 shows the expected punch-through contribution. As seen, it is small compared to the continuum. We note that similar calculations were made for experiment R209, and the results agree with the predictions.

9.3 Hadron decay

The decay path for hadrons is a factor of ~ 4 times shorter here than what we have at the ISR, while the average momentum per track is expected to be larger. For pions, the decay probability is $(0.3/p_T)\%$, with p in GeV, or 7×10^{-5} for 40 GeV π's. For kaons it is $(2/p_T)\%$, or 5×10^{-4} for 40 GeV K's.

Using the hadron production formula described above, we have computed the hadron decay contribution to muon pair, shown in Fig. 13. It is found to be negligible.

9.4 QED contribution

We have also looked into the possibility of a pair of back-to-back high-energy π^0's each converting asymmetrically in the high-Z absorber into one energetic muon and one soft muon, and thus creating a pair of high-mass muons. Using the Bethe-Heitler cross-section, we have calculated that this process is negligible.

Figure 13 summarizes the computed background coming from all three processes. As seen, the background is small compared to the continuum above a mass of 30 GeV and is totally negligible compared to the expected Z^0 yield.

10. SEARCH FOR $W^{\pm}$

The production of $W^{\pm}$ [9-11] and its decay to $\mu + \nu$ has been discussed in detail by many physicists. It is generally believed that the $\mu^{\pm}$ from W decays have a sufficiently high p_T (which is approximately 1/2 m_W) so that they can easily be detected. The mass of $W^{\pm}$ is supposed to be less than that of Z^0. The hadron decay background and the hadron punch-through are much larger in this case as compared to $Z^0 \to \mu^+\mu^-$. In Fig. 14 we computed the $W^{\pm} \to \mu^{\pm}\nu$ decay and various hadron backgrounds in the same way as before. It is obvious that the detector can easily see a $W^{\pm}$ signal. The total number of events is about 600.

Since the detector covers small muon angles (20°), where the charge asymmetry for $W^+ \to \mu^+\nu$ and $W^- \to \mu^-\bar{\nu}$ gives two unique signatures, they can also be easily measured, as shown in Fig. 15.

11. PATTERN RECOGNITION AND DATA ANALYSIS

It took us less than six months to convert the ISR muon analysis program to the PETRA experiment. The present experiment is similar to the two previous experiments in size, geometry, and technique, i.e. all with a configuration of absorber-drift chamber-absorber-counter (time-of-flight)-chamber. We do not expect it to take more than one year to convert our present ISR-PETRA program to the new $\bar{p}p$ experiment.

Based on our experience at the ISR (see Fig. 2), we expect that very few tracks in the outside muon chambers will not be due to muons. To select muon events off-line, we therefore demand that, in the outside chambers, each muon candidate be associated with one line pointing back to the intersection region. That line should also be in the same sector as the trigger counter and be consistent with TOF measurements of the counters. Furthermore, in that sector we require more than 50 wires to be fired in the inner projection chamber. To select high p_T particles, we also require the mean TOF of the i^{th} and the $(120-i)^{th}$ wires in the sector to be within 200 nsec of the mean value of all the wires, i.e.

$$\left|\frac{T_i + T_{120-i}}{2} - \left\langle T_i \right\rangle\right| < 200 \text{ nsec} .$$

This cut effectively sets a lower-limit cut of 5 GeV in the p_T of the particles. Since we expect less than 0.1 hadrons produced with $p_T > 5$ GeV per second after the absorber, the data rate after the requirement of TOF cut will be very low, i.e. less than 0.1/sec even for a single-muon trigger. Only for events satisfying this condition will we have to fit for the momentum in the central chamber and project the trajectory outward through the return yoke to check the matching of the fitted trajectory with the measured line in the outside muon chambers, and also to project inward through the absorber to check the vertex. Background events of the nature of hadron punch-through or decay will be rejected by these checks. The fitting process will consume about 1 cpu second per event for the

CDC 7600 computer. Therefore, the total computing requirement will be about 100 hours of the CDC computer time per year. We view the simplicity of the trigger, the data reduction, and momentum analysis of the events as the major features of the proposed detector.

12. SUMMARY

As we have discussed in this proposal, this is a detector with a definite goal.

We have designed this detector based on our previous experiences with detectors of a similar kind to measure muon pairs. The present detector will enable us to continue our search for new particles up to the highest possible mass.

Table 1 shows our preliminary plans to build up this detector. We are aware that many physicists may be interested in similar projects and we welcome possible future collaborators.

The previous two detectors at PETRA and the ISR were of about the same size and perhaps more complexity. They were both built and operated in data-taking mode within 18 months, and we have no reason to suspect that we will be seriously delayed in our present effort.

Finally, if approved, we will be able to use the full luminosity of 10^{30} cm^{-2} s^{-1} at the beginning of 1981. A low-β insertion by that time is therefore most important.

13. OTHER POSSIBILITIES

It should be obvious to everyone that the detector can easily be modified to study hadron physics, such as multiplicity, total cross-section, high p_T, correlation, and so forth, once the central absorber is removed. Other possibilities may also exist if one measures the dE/dx on each drift wire as in the TPC or the JADE chambers.

This physics program can be undertaken even with luminosity as low as 10^{27} cm^{-2} s^{-1}.

Table 1

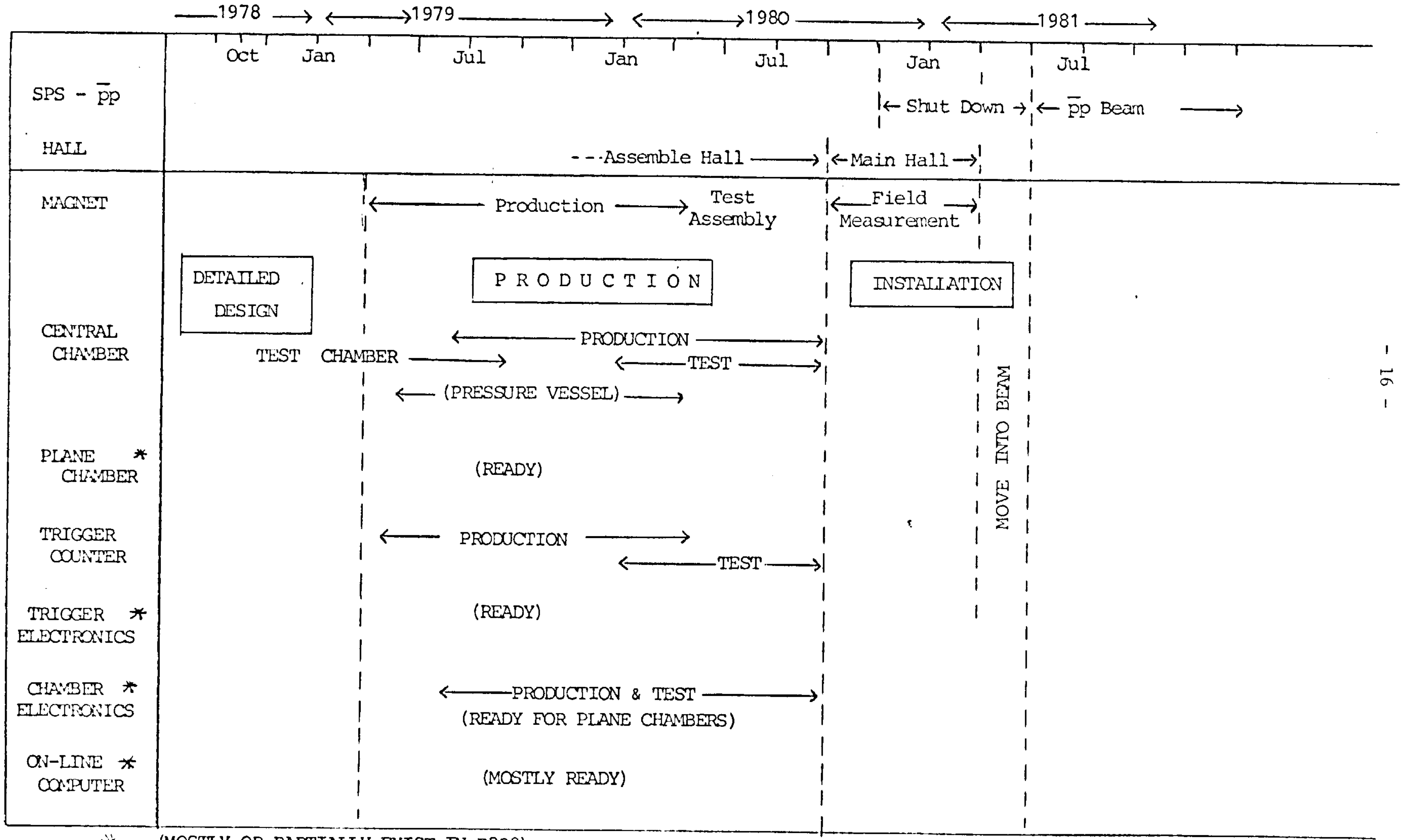

* (MOSTLY OR PARTIALLY EXIST IN R209)

MAGNET	YOKES (+)	
	COIL	
	POWER SUPPLY	
	COOLING	
	MAGNET SUPPORT	
ABSORBER		
CHAMBERS	CENTRAL CYLINDRICAL DRIFT CHAMBER (WITH PRESSURE VESSEL)	
	PLANE DRIFT CHAMBERS (+) (WITH SUPPORTS)	
	GAS SYTEM	
	HV POWER SUPPLY	
	PRE AMP.	
	CABLES	
TRIGGER COUNTERS	COUNTERS	
	TUBES, BASES, HOUSING, SUPPORTS	
	HV POWER SUPPLY	
	CABLES	
TRIGGER ELECTRONICS (+)	DISCRIMINATORS (MEAN TIMERS)	HUT WITH AIR-CONDITIONING
	TRIGGER BOX	
	TDC's	
	ADC's	
	SCALERS	
CHAMBER ELECTRONICS	MULTI-HIT TDC's (FOR CENTRAL CHAMBER)	NIM, CAMAC CRATES
	TDC's (2770) (+) (FOR PLANE CHAMBERS)	
	TRACK FINDER	LEMO, BNC CABLES
	CALIBRATION SYSTEM FOR TDC's	
ON-LINE COMPUTER (+)	COMPUTER(S) WITH PERIPHERALS	
	MICRO PROCESSOR(S) - MBD-	
	CDC/IBM LINK	

(+) MOSTLY EXIST. IN R209

REFERENCES and FOOTNOTES

1) C. Rubbia, P. McIntyre and D. Cline, Proc. Internat. Neutrino Conf., Aachen, 1976, p. 683.

2) $p\bar{p}$ Study Week CERN, 28 March-2 April, 1977.

3) D. Antreasyan et al., Measurement of high-mass muon pairs at high energies, 19th Internat. Conf. on High-Energy Physics, Tokyo, 1978.

4) S.D. Drell and T.M. Yan, Phys. Rev. Letters 25, 316 (1970).

5) K. Kinoshita, H. Satz and D. Schildknecht, Bielefeld University Report, BI-TP 77/14 (1977).

6) S.W. Herb et al., Phys. Rev. Letters 39, 252 (1977).

7) MARK-J Proposal at PETRA (1976).

8) This device was a copy of the design at CERN by M. Pizer and his group.

9) R.F. Peierls et al., Phys. Rev. 16, 1397 (1977).

10) C. Quigg, Rev. Mod. Phys. 44, 297 (1977).

11) M. Perrottet, HUTP 77/A048.

12) JADE Proposal for a compact magnetic detector at PETRA.

13) W. Farr et al., Nuclear Instrum. Methods 154, 175 (1978).

14) We would like to acknowledge detailed discussions with T. Taylor at CERN.

15) U. Becker et al., Nuclear Instrum. Methods 128, 593 (1975).

16) R.L. Gluckstern, Nuclear Instrum. Methods 24, 381 (1963).

17) F.W. Büsser et al., Nuclear Phys. B106, 1 (1976), and private communication from L. Camilleri.

Figure captions

Fig. 1 : Plan view of the muon pair detector at the ISR by the Pisa-Naples-Frascati-Harvard-CERN-LAPP-MIT Collaboration.

Fig. 2 : Schematic view of a reconstructed event obtained in the ISR experiment:

a) 14 tracks seen in the inner detector;
b) only muon tracks appear in chambers after absorber.

Fig. 3 : Dimuon mass spectrum from the ISR experiment. The line represents a 0 parameter fit obtained by scaling the Fermilab data, also plotted for comparison.

Fig. 4 : Side view (a) and end view (b) of the Mark-J detector at PETRA.

Fig. 5 : a) Side view of the proposed detector.
b) Same view, enlarged.

Fig. 6 : a) End view of the proposed detector.
b) Same view, enlarged.

Fig. 7 : Schematic view of the chamber element developed for the JADE experiment at PETRA.

Fig. 8 : Picture of the end-plate of the pressure vessel used for the JADE chambers.

Fig. 9 : Arrangement of the different counter hodoscopes.

Fig. 10 : Partial block diagram of the trigger logic.

Fig. 11 : a) Variation of the mass resolution as a function of the polar angle of one muon.

b) Acceptance of detector for muon pairs. Both the total acceptance and the "very high resolution" acceptance are shown. The production and decay distribution assumed is

$$\frac{d^2\sigma}{dX_f \, d(\cos \theta^*)} = (1 - X_f)^3 \, \{1 + \cos^2 (\theta)\}.$$

where $X_f \approx 2p_L/\sqrt{s}$ and θ^* is the polar angle of one of the muons in the dimuon rest frame.

Fig. 12 : Cross-sections expected for dimuon continuum production and Z^0 production. The gain coming from an antiproton beam instead of a proton beam is also shown. The corresponding scale is shown on the right side.

The $Z^0 \rightarrow \mu^+\mu^-$ cross-section is taken from Ref. 9, assuming a branching ratio of 5%.

Fig. 13 : Computed background coming from hadron punch-through and hadron decays. The Z^0 signal is shown for comparison. For hadron decays the decay path is taken equal to 15 cm and all particles are assumed to be kaons.

Fig. 14 : Computed cross-section for the $W^{\pm} \rightarrow \mu^{\pm}\nu$ for a mass m_W = 70 GeV/c^2. Backgrounds from hadron decay and punch-through are also shown.

Fig. 15 : Number of events obtained after 300 hours for the decay $W^{\pm} \rightarrow \mu^{\pm}\nu$ as a function of cos θ; θ being the polar angle of emission of the single muon.

$p + p \rightarrow M + X$

$\quad \hookrightarrow \mu^+ + \mu^-$

$m_J < \text{mass} < 60 \text{ GeV}$

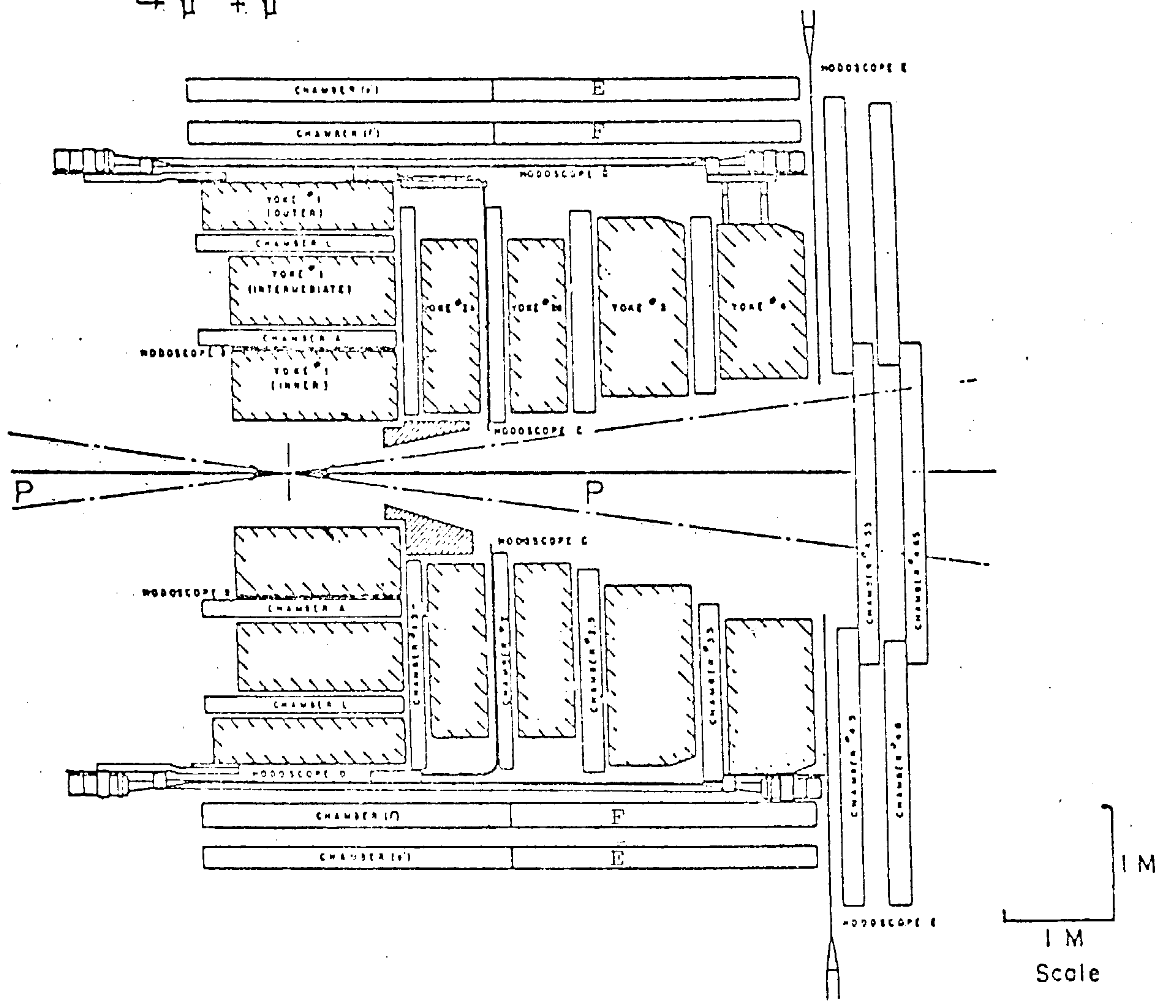

Fig. 1

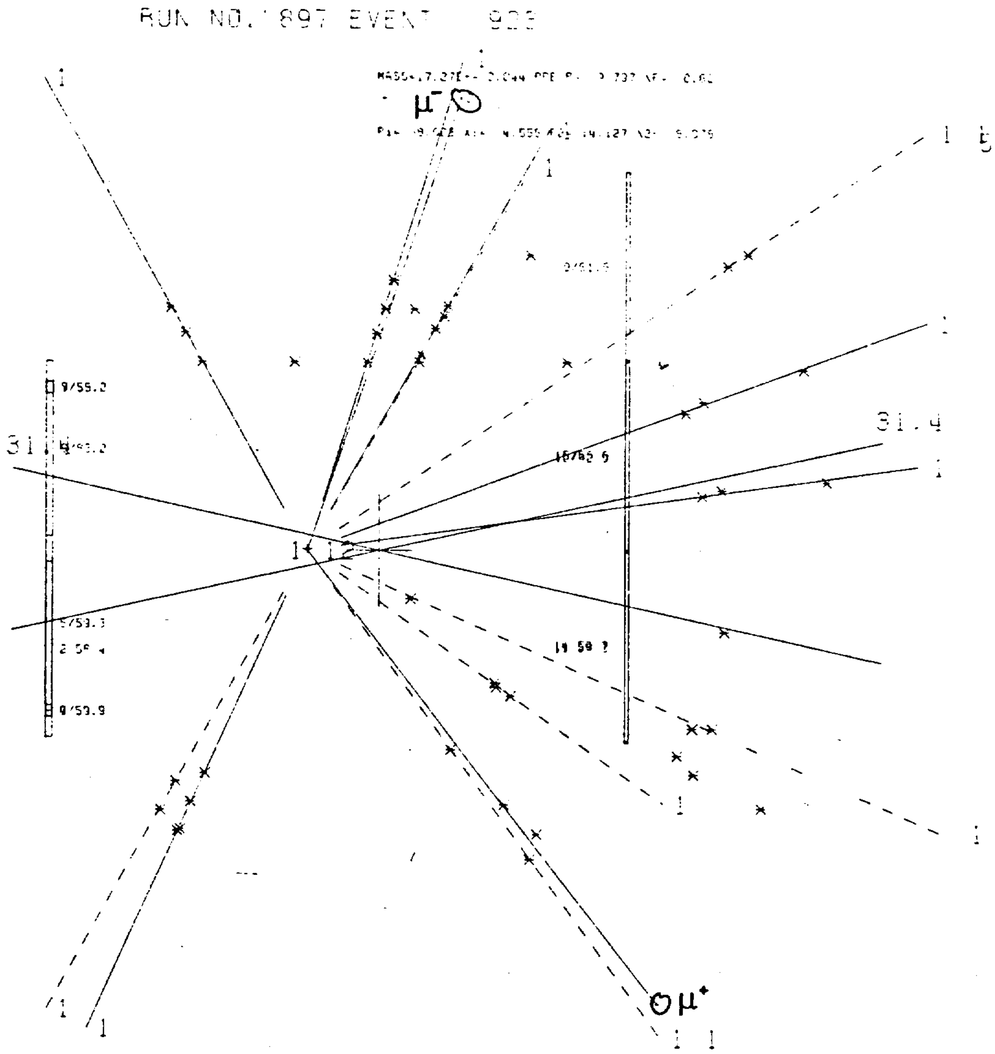

Fig. 2a

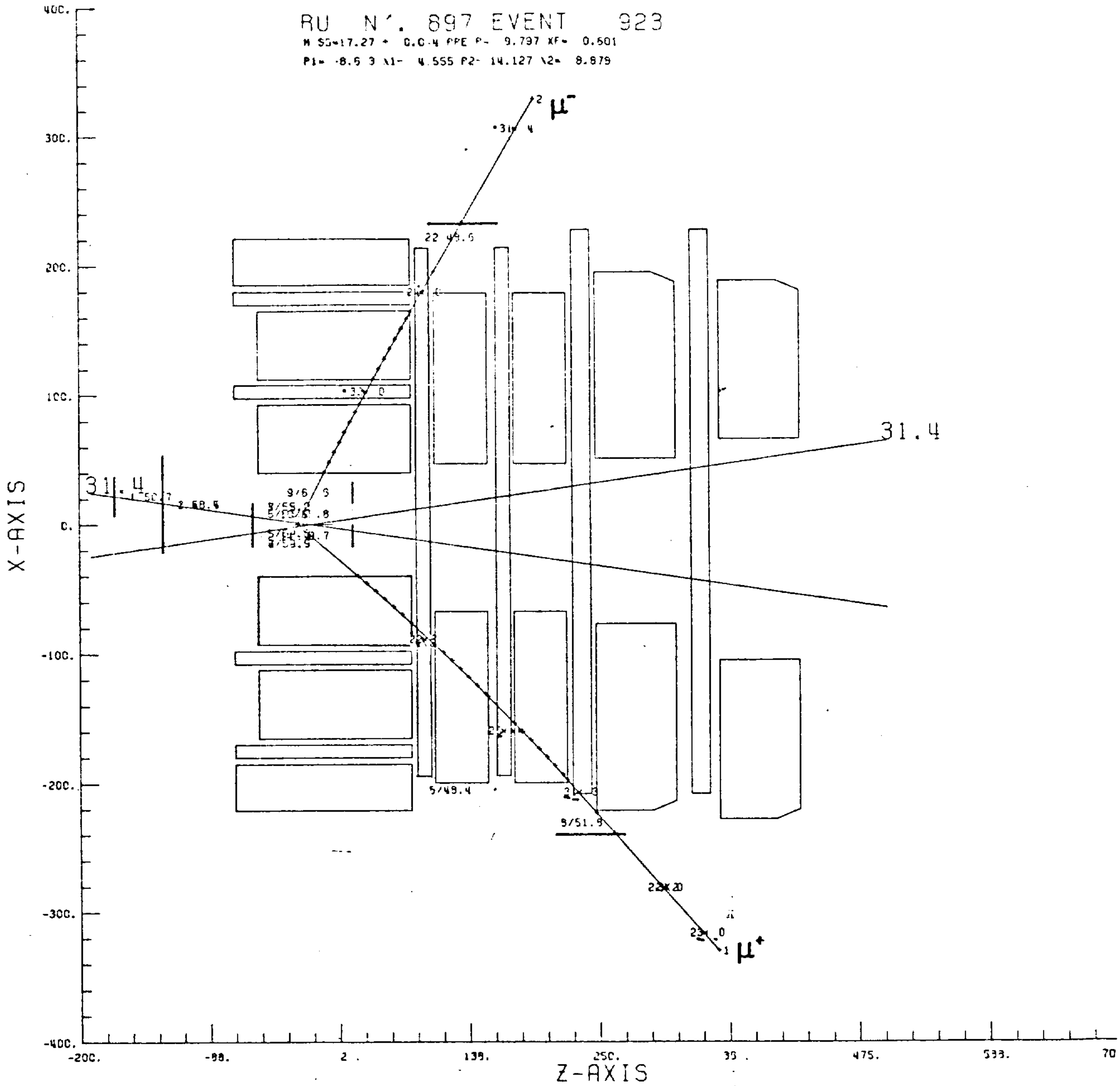

Fig. 2b

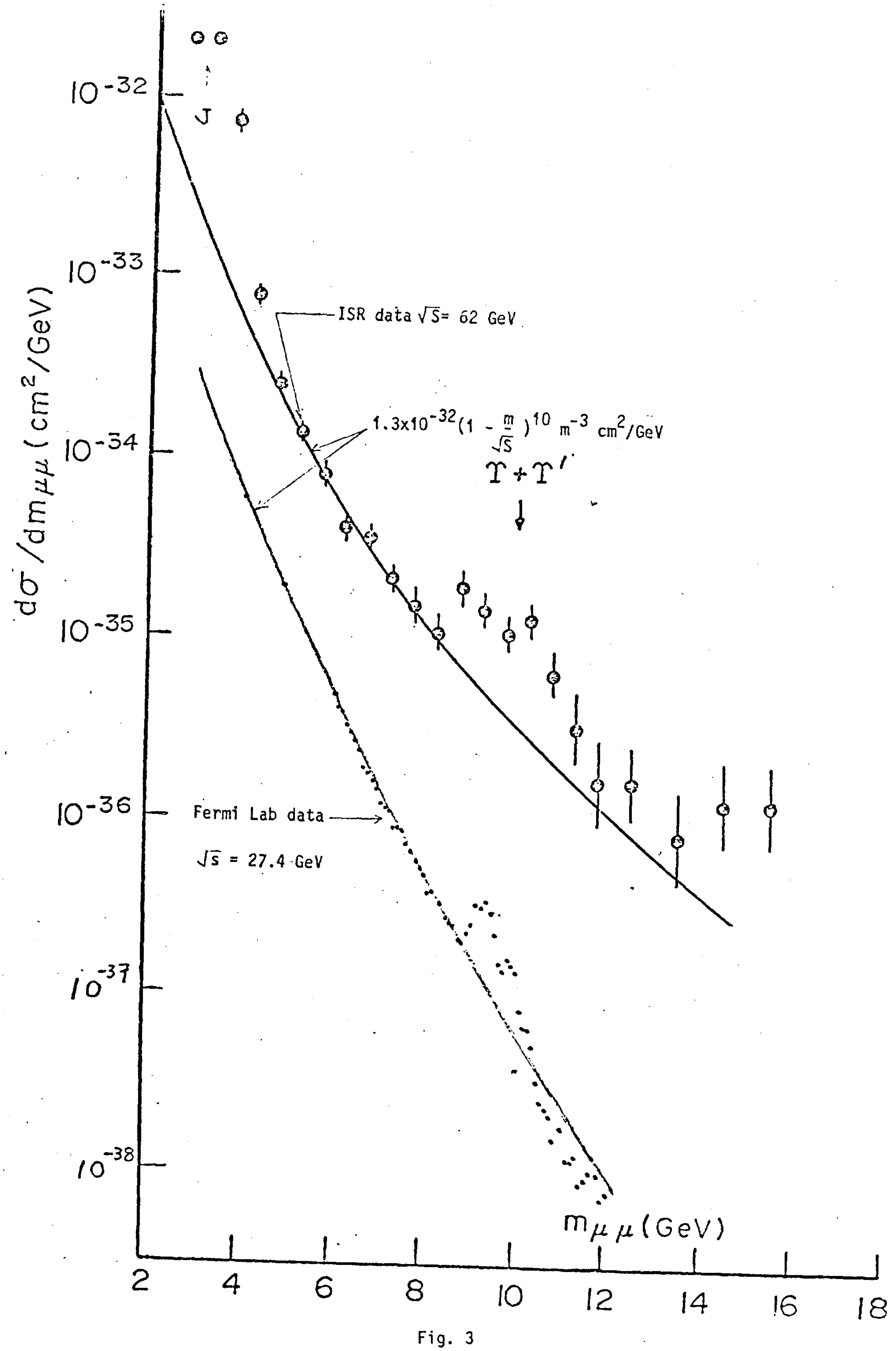

10^{-32}
10^{-33}
10^{-34}
10^{-35}
10^{-36}
10^{-37}
10^{-38}
$d\sigma/dm_{\mu\mu}$ (cm^2/GeV)
J
ISR data $\sqrt{s}$= 62 GeV
$1.3\times10^{-32}(1-\frac{m}{\sqrt{s}})^{10}\ m^{-3}$ cm^2/GeV
$\Upsilon+\Upsilon'$
Fermi Lab data
$\sqrt{s}$ = 27.4 GeV
$m_{\mu\mu}$ (GeV)
2
4
6
8
10
12
14
16
18

Fig. 3

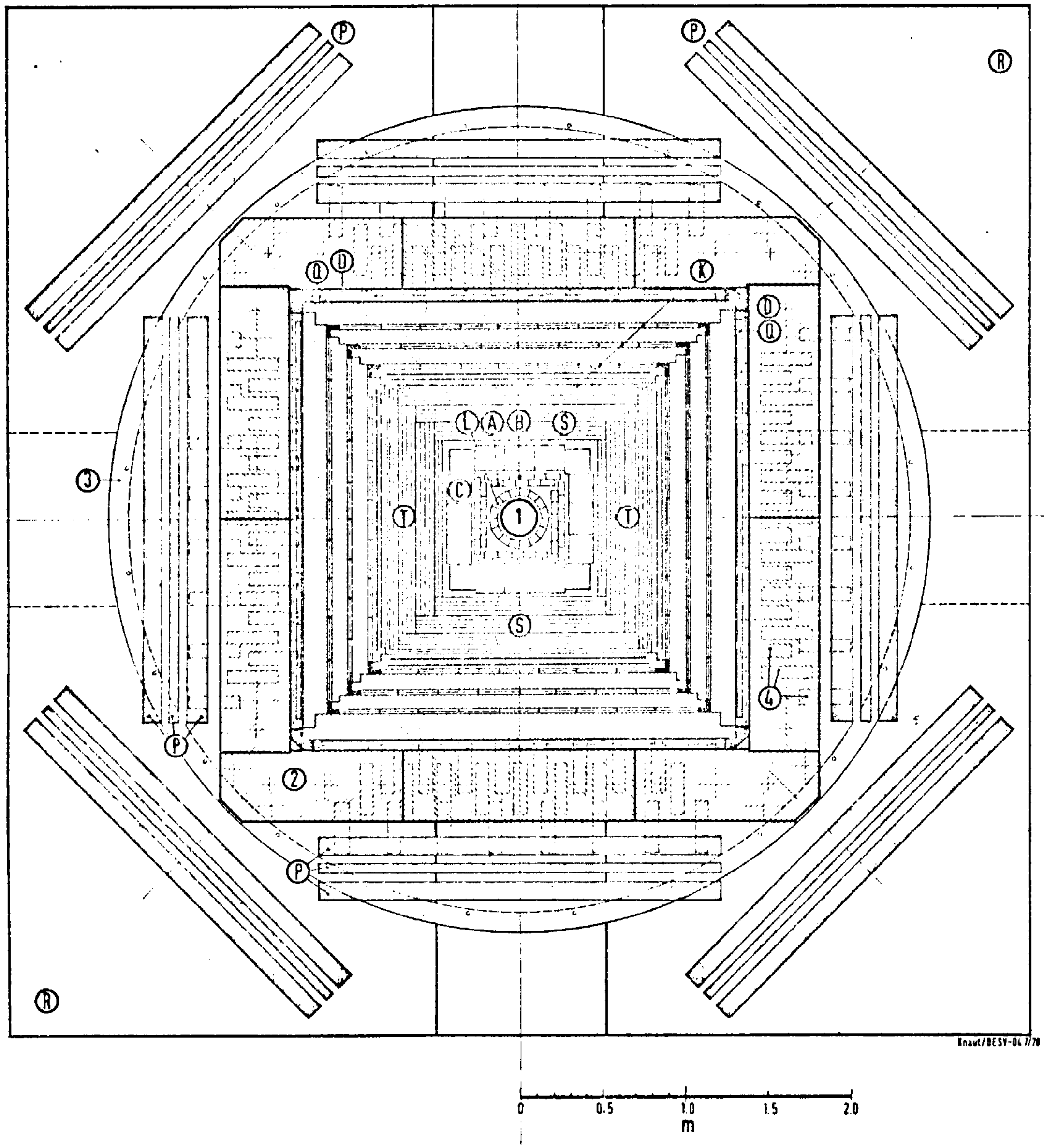
MARK J-DETECTOR
(Cross Section)
ⒶⒷⒸ SHOWER COUNTERS
Ⓓ TRIGGER COUNTERS
Ⓛ LUCITE TRIGGER COUNTERS
Ⓠ DRIFT CHAMBERS, MEDIAN
ⓅⓇ DRIFT CHAMBERS, OUTER
ⓈⓉ DRIFT CHAMBERS, INNER
① BEAM PIPE
② MAGNET IRON
③ Al-RING
④ MULTIPLIERS
WEIGHT (total) : ~ 400 t
MAGNETIC FIELD: 1.8 T
PARTICIPANTS:
RWTH - Aachen
DESY - Hamburg
MIT - Cambridge
NIKHEF - Amsterdam
HEPI - Peking
0
0.5
1.0
1.5
2.0
m

Fig. 4a

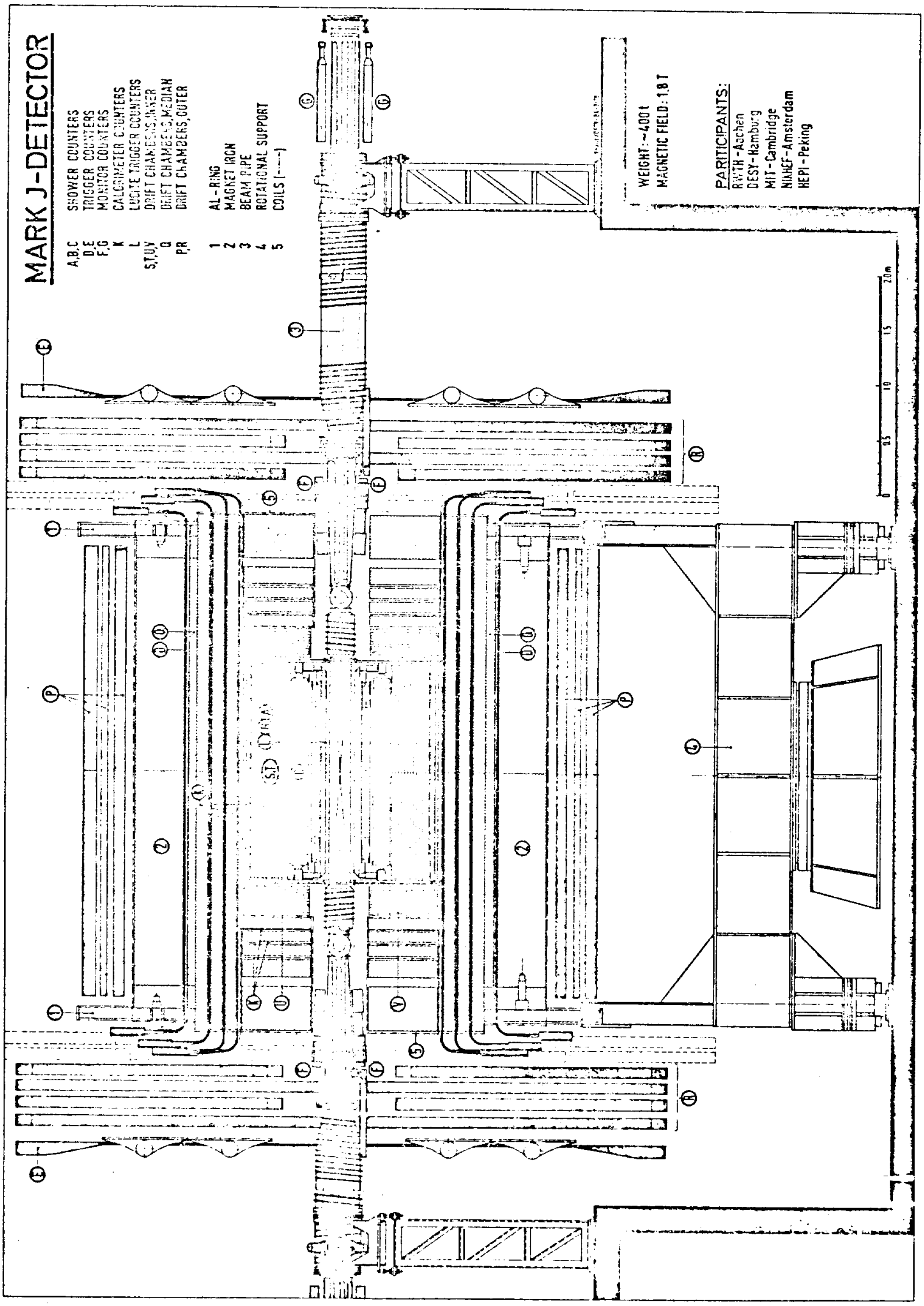
MARK J-DETECTOR
A,B,C SHOWER COUNTERS
D,E TRIGGER COUNTERS
F,G MONITOR COUNTERS
K CALORIMETER COUNTERS
L LUCITE TRIGGER COUNTERS
S,T,U,V DRIFT CHAMBERS,INNER
Q DRIFT CHAMBERS,MEDIAN
P,R DRIFT CHAMBERS,OUTER
1 AL-RING
2 MAGNET IRON
3 BEAM PIPE
4 ROTATIONAL SUPPORT
5 COILS (---)
WEIGHT: ~400 t
MAGNETIC FIELD: 1.8 T
PARITICIPANTS:
RWTH-Aachen
DESY-Hamburg
MIT-Cambridge
NIKHEF-Amsterdam
HEPI-Peking

Fig. 4b

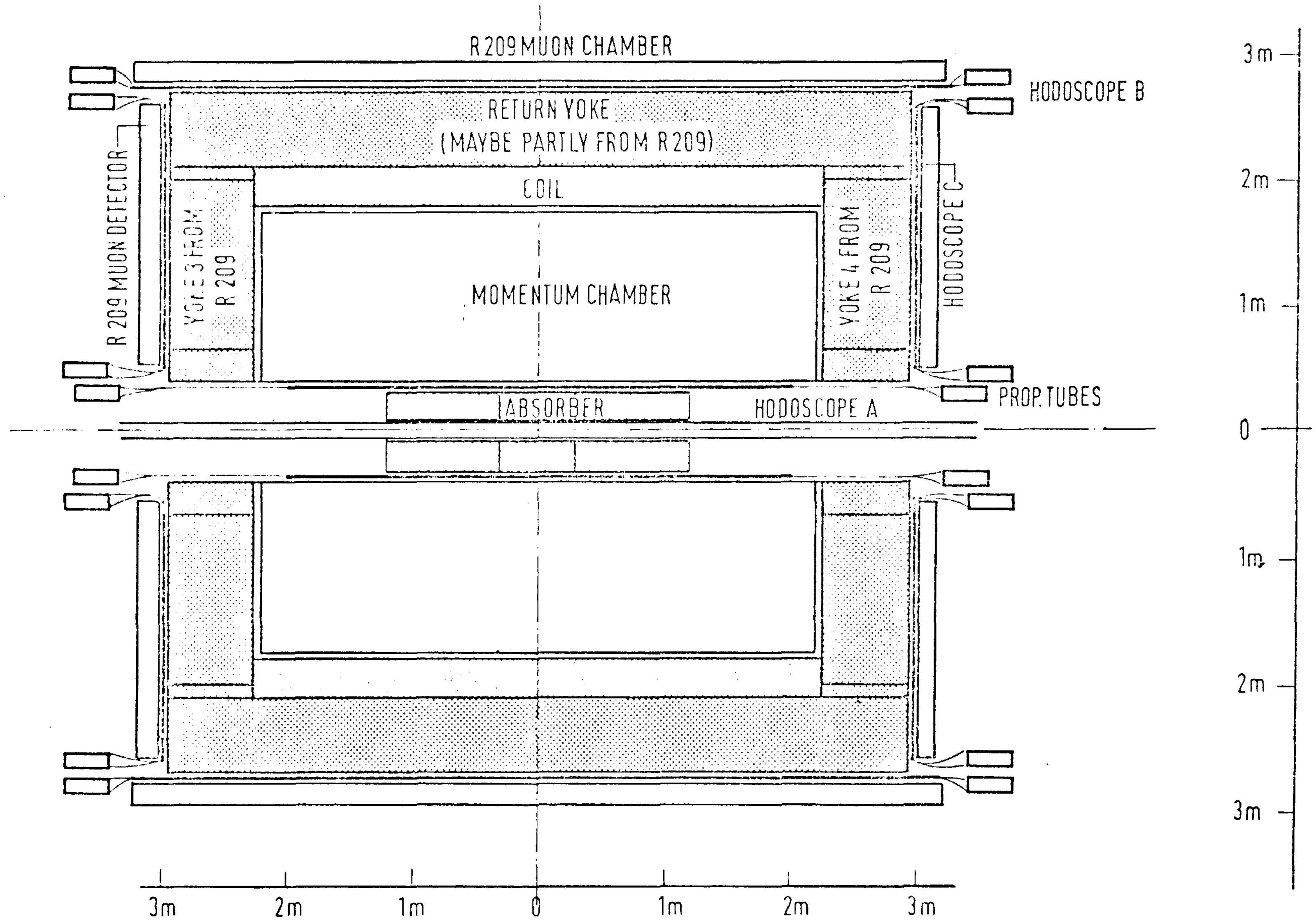

SIDE VIEW OF THE PROPOSED DETECTOR

Fig. 5a

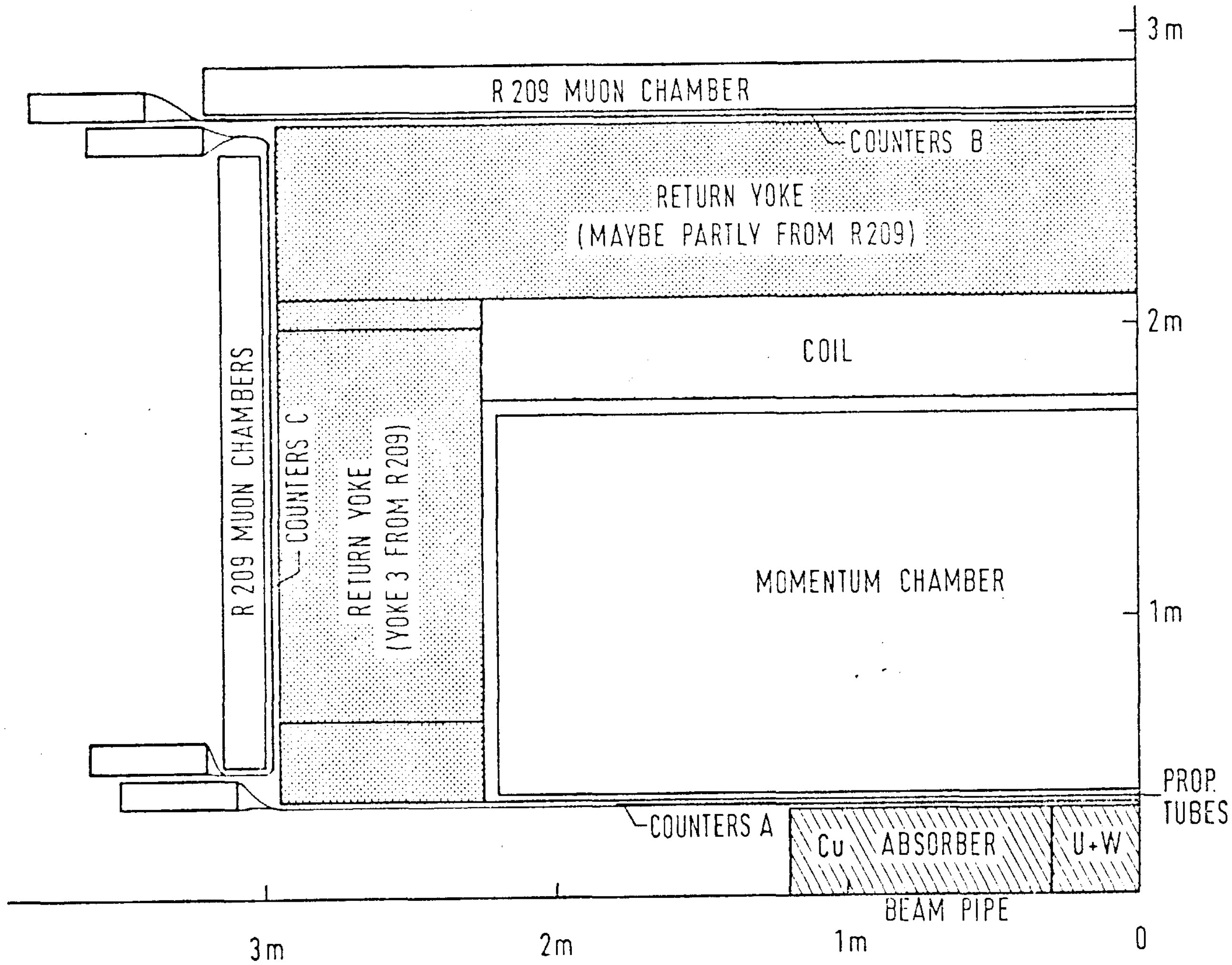
3 m
R 209 MUON CHAMBER
COUNTERS B
RETURN YOKE
(MAYBE PARTLY FROM R209)
2 m
COIL
R 209 MUON CHAMBERS
COUNTERS C
RETURN YOKE
(YOKE 3 FROM R209)
MOMENTUM CHAMBER
1 m
PROP. TUBES
COUNTERS A
Cu ABSORBER
U+W
BEAM PIPE
3 m
2 m
1 m
0

Fig. 5b

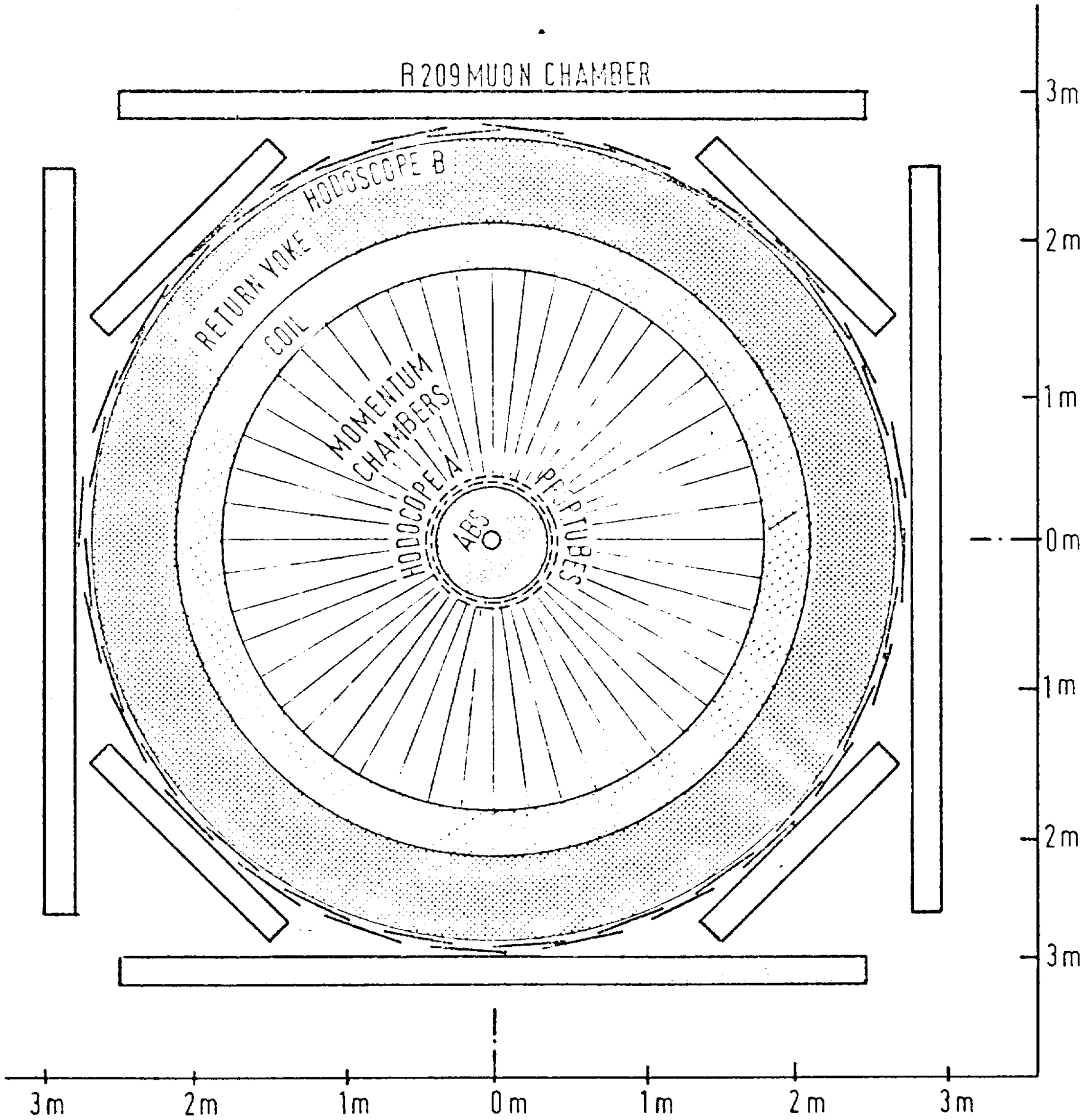

END VIEW OF THE PROPOSED DETECTOR

Fig. 6a

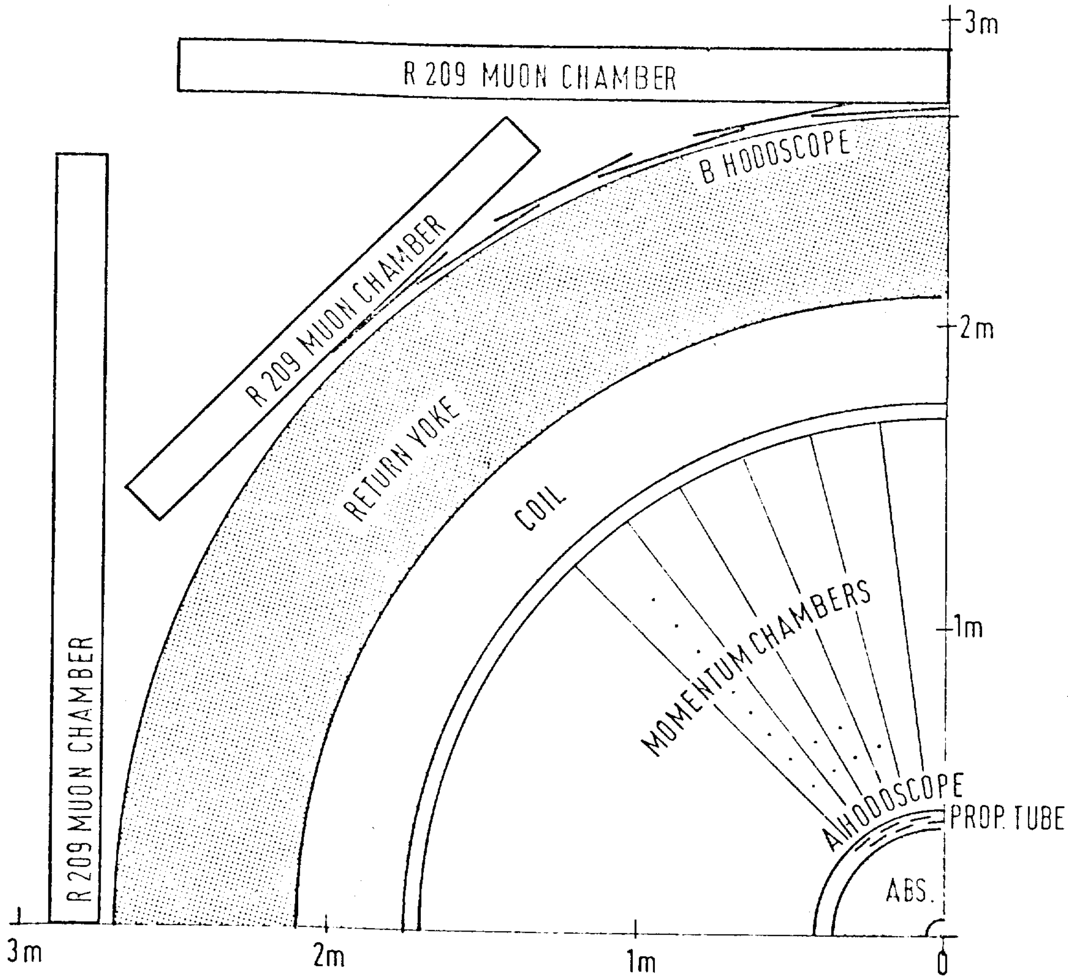

R 209 MUON CHAMBER
R 209 MUON CHAMBER
R 209 MUON CHAMBER
B HODOSCOPE
RETURN YOKE
COIL
MOMENTUM CHAMBERS
A HODOSCOPE
PROP. TUBE
ABS.
3m
2m
1m
0

Fig. 6b

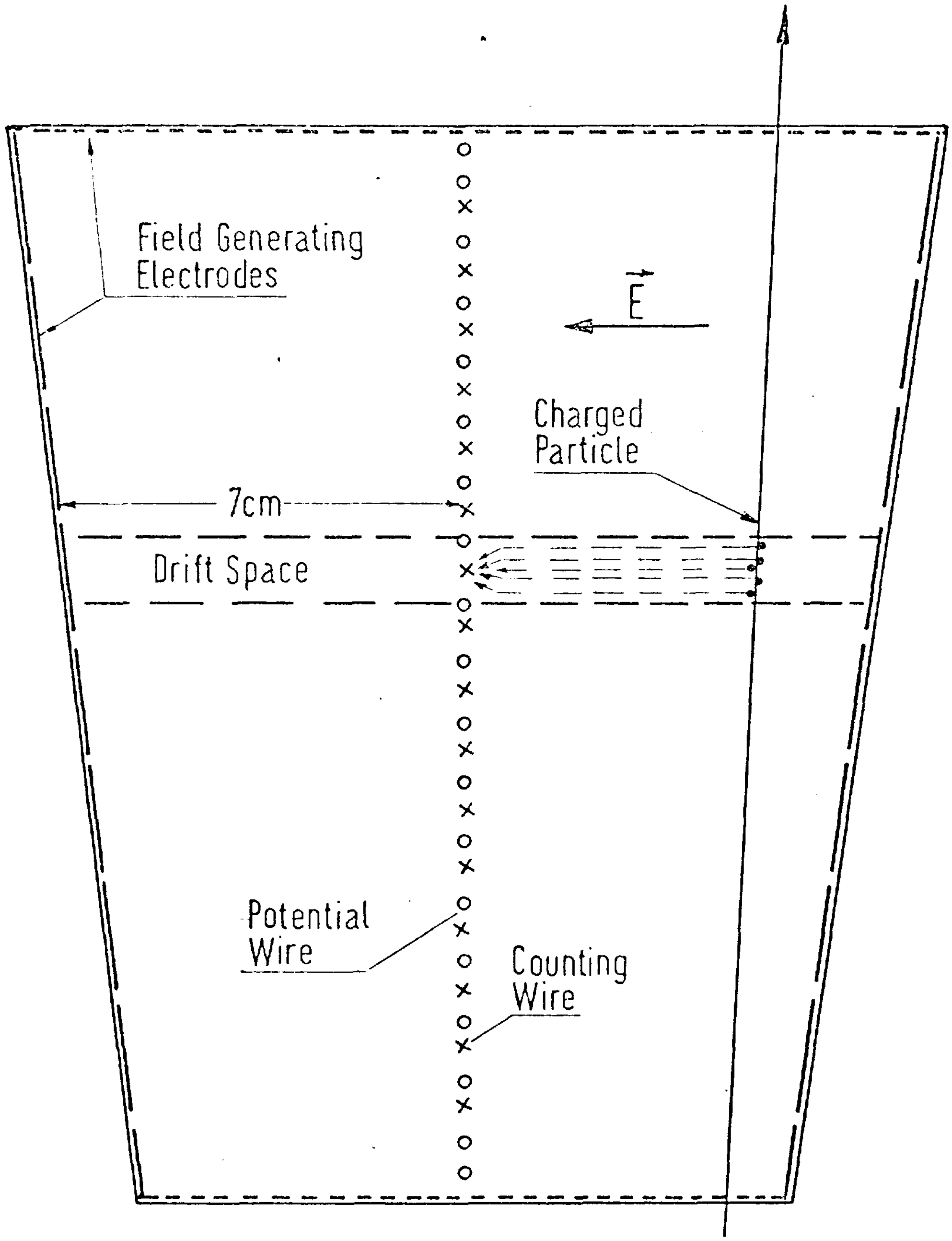

Field Generating
Electrodes
E
Charged
Particle
7cm
Drift Space
Potential
Wire
Counting
Wire

Fig. 7

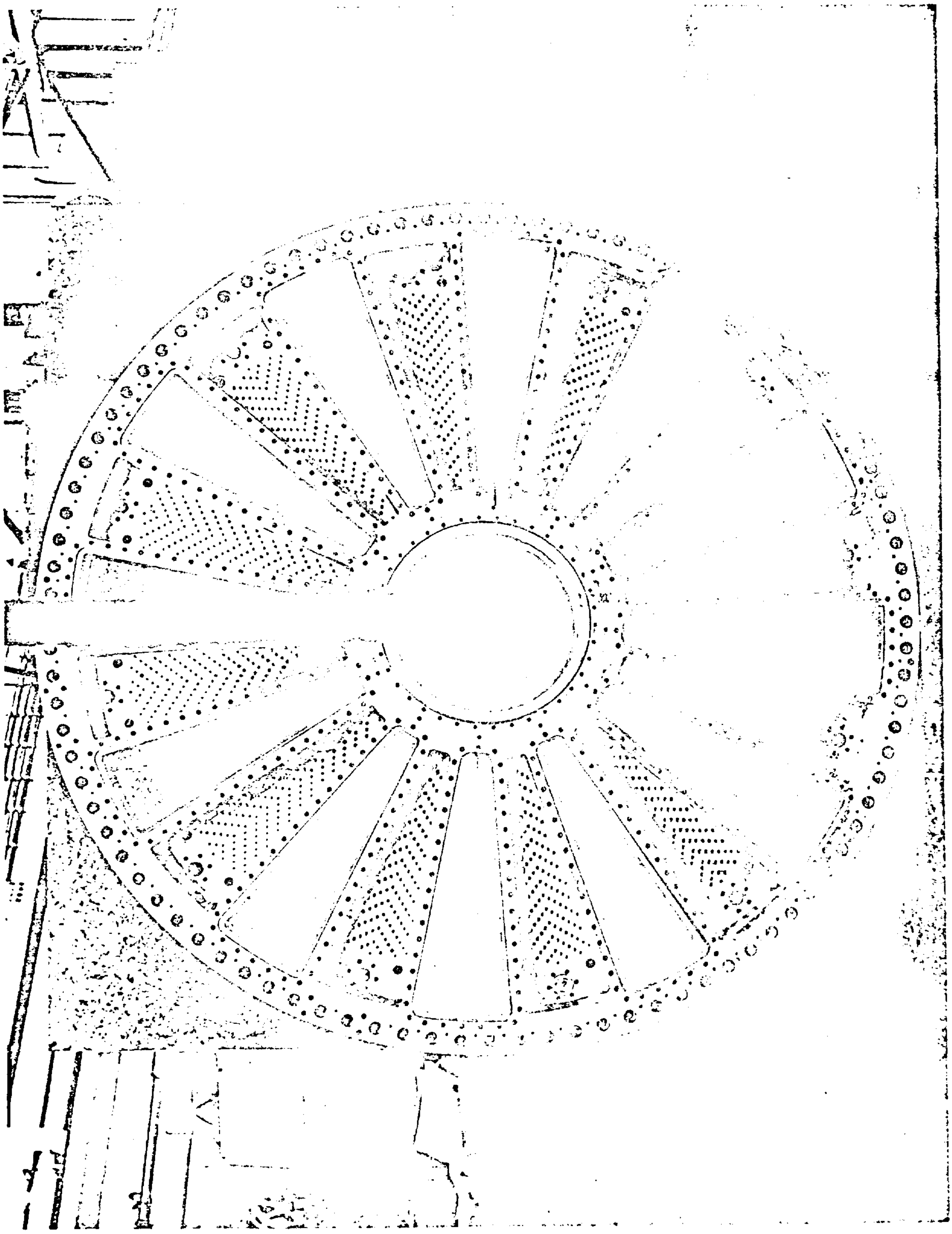

Fig. 8

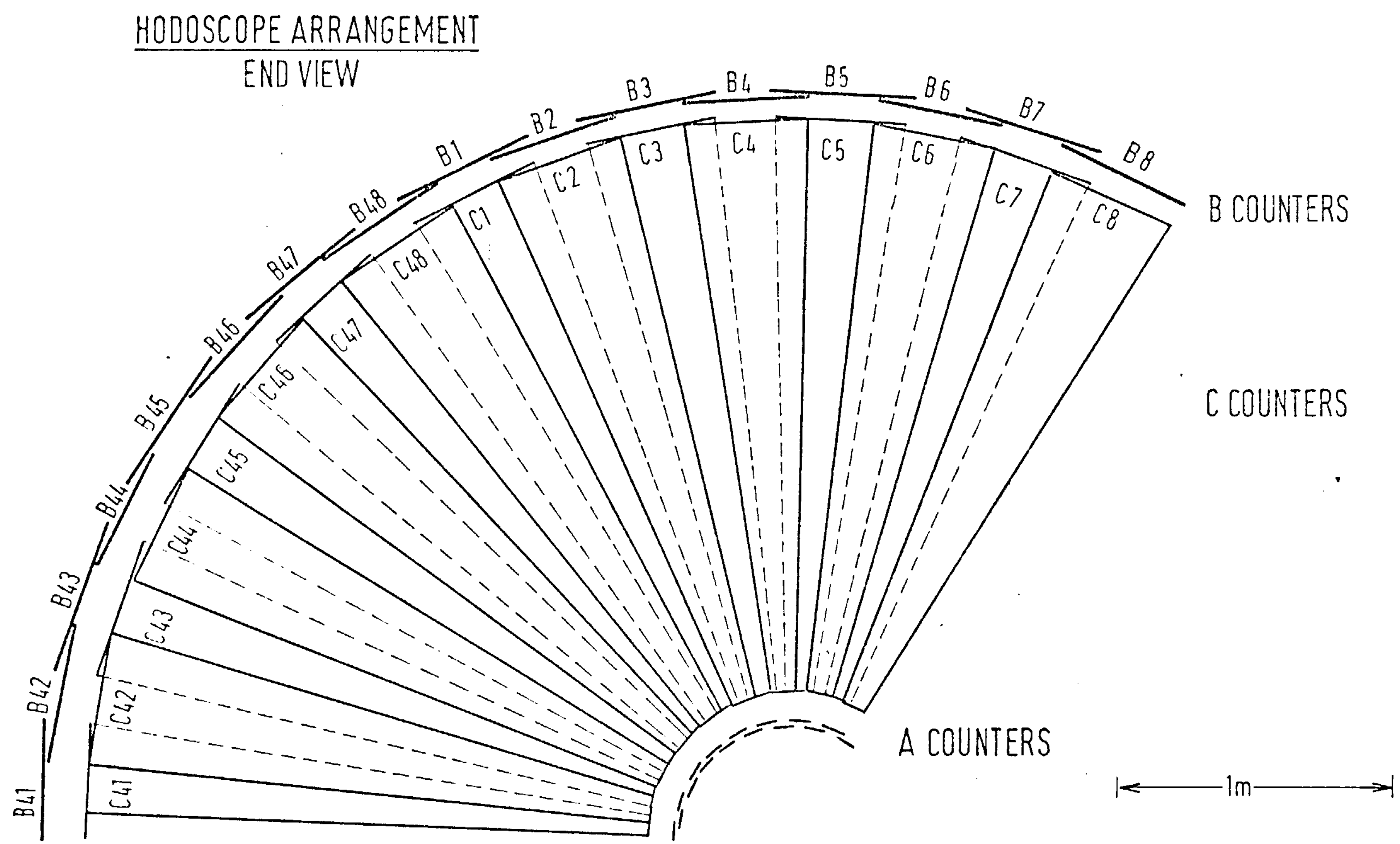
HODOSCOPE ARRANGEMENT
END VIEW
B41
B42
B43
B44
B45
B46
B47
B48
B1
B2
B3
B4
B5
B6
B7
B8
C41
C42
C43
C44
C45
C46
C47
C48
C1
C2
C3
C4
C5
C6
C7
C8
B COUNTERS
C COUNTERS
A COUNTERS
1m

Fig. 9

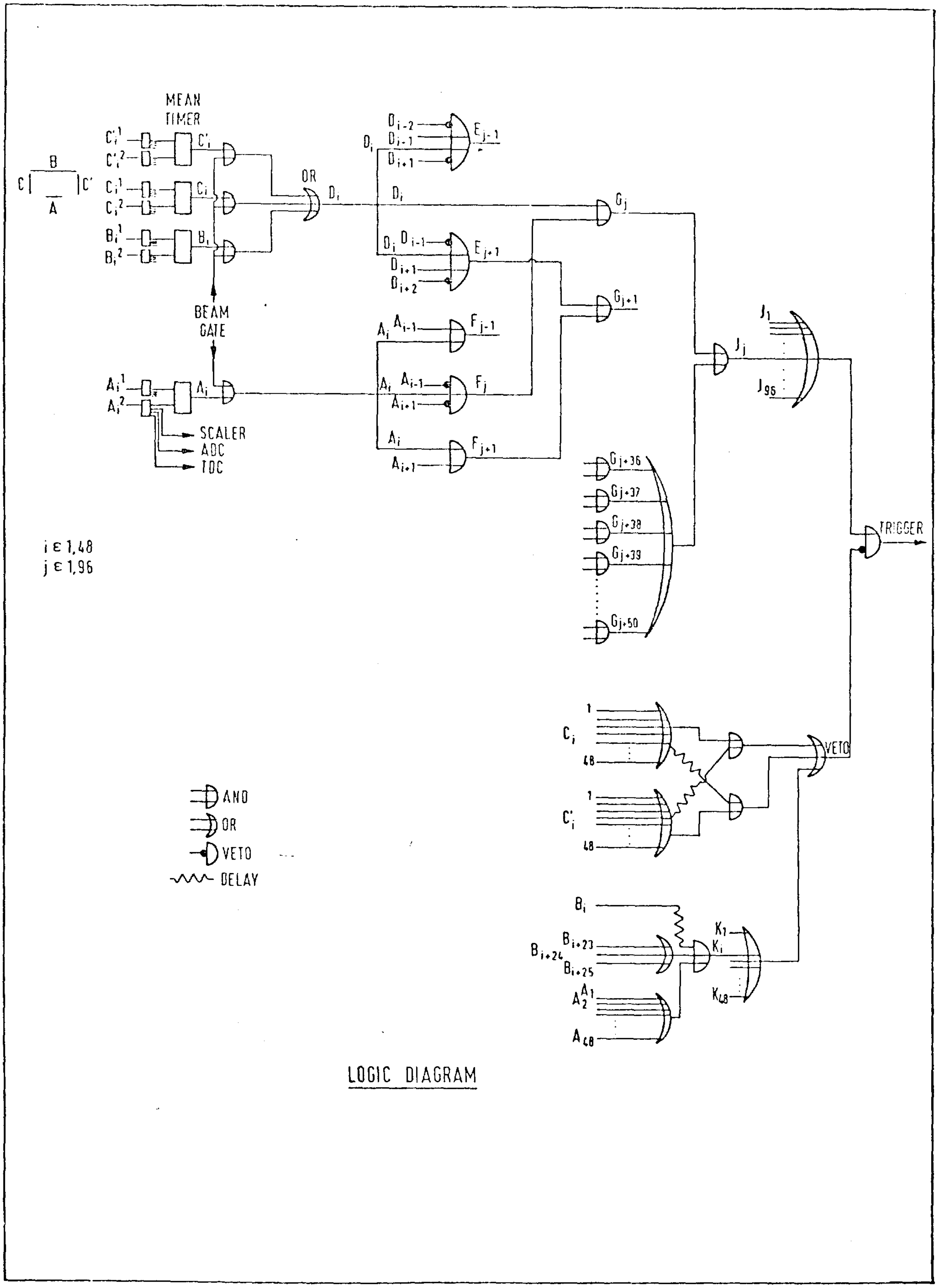
MEAN TIMER
OR
BEAM GATE
SCALER
ADC
TDC
TRIGGER
VETO
i ε 1,48
j ε 1,96
AND
OR
VETO
DELAY
LOGIC DIAGRAM

Fig. 10

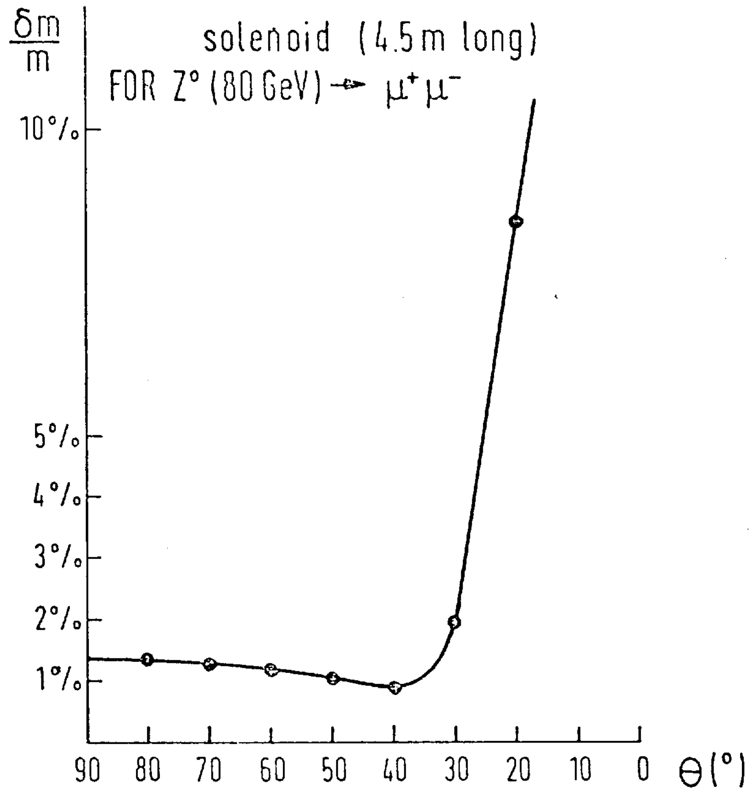
$\frac{\delta m}{m}$
solenoid (4.5 m long)
FOR Z° (80 GeV) $\rightarrow \mu^+\mu^-$
10°/o
5°/o
4°/o
3°/o
2°/o
1°/o
90
80
70
60
50
40
30
20
10
0
Θ(°)

Fig. 11a

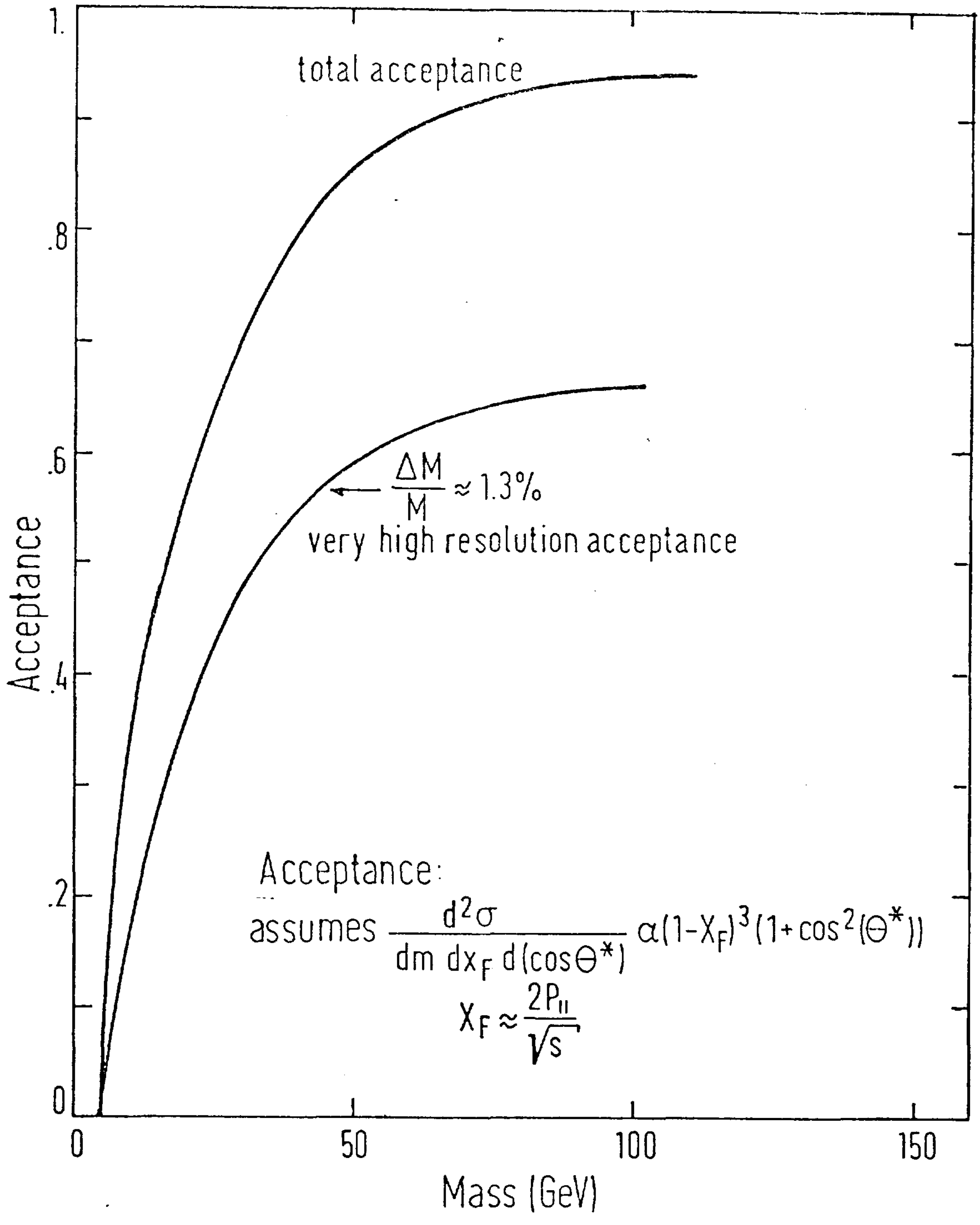

total acceptance
$\frac{\Delta M}{M} \approx 1.3\%$
very high resolution acceptance
Acceptance:
assumes $\frac{d^2\sigma}{dm\, dx_F\, d(\cos\Theta^*)} \alpha (1-X_F)^3(1+\cos^2(\Theta^*))$
$X_F \approx \frac{2P_{\parallel}}{\sqrt{s}}$
Acceptance
1.
.8
.6
.4
.2
0
0
50
100
150
Mass (GeV)

Fig. 11b

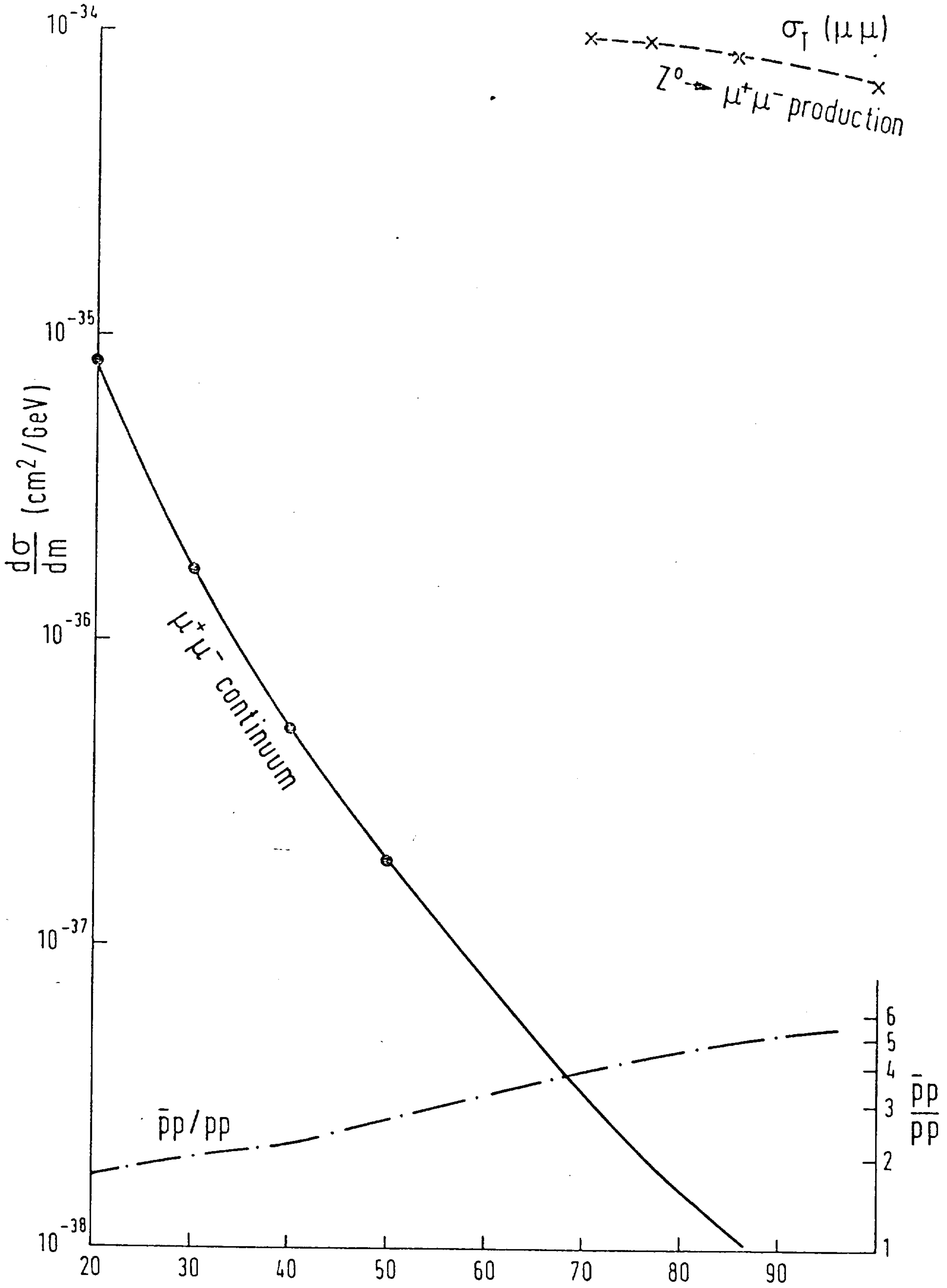
σ_T ($\mu\mu$)
$Z^0 \to \mu^+\mu^-$ production
$\mu^+\mu^-$ continuum
$\bar{p}p/pp$
$\frac{d\sigma}{dm}$ (cm^2/GeV)
10^{-34}
10^{-35}
10^{-36}
10^{-37}
10^{-38}
20 30 40 50 60 70 80 90
1 2 3 4 5 6
$\frac{\bar{p}p}{pp}$

Fig. 12

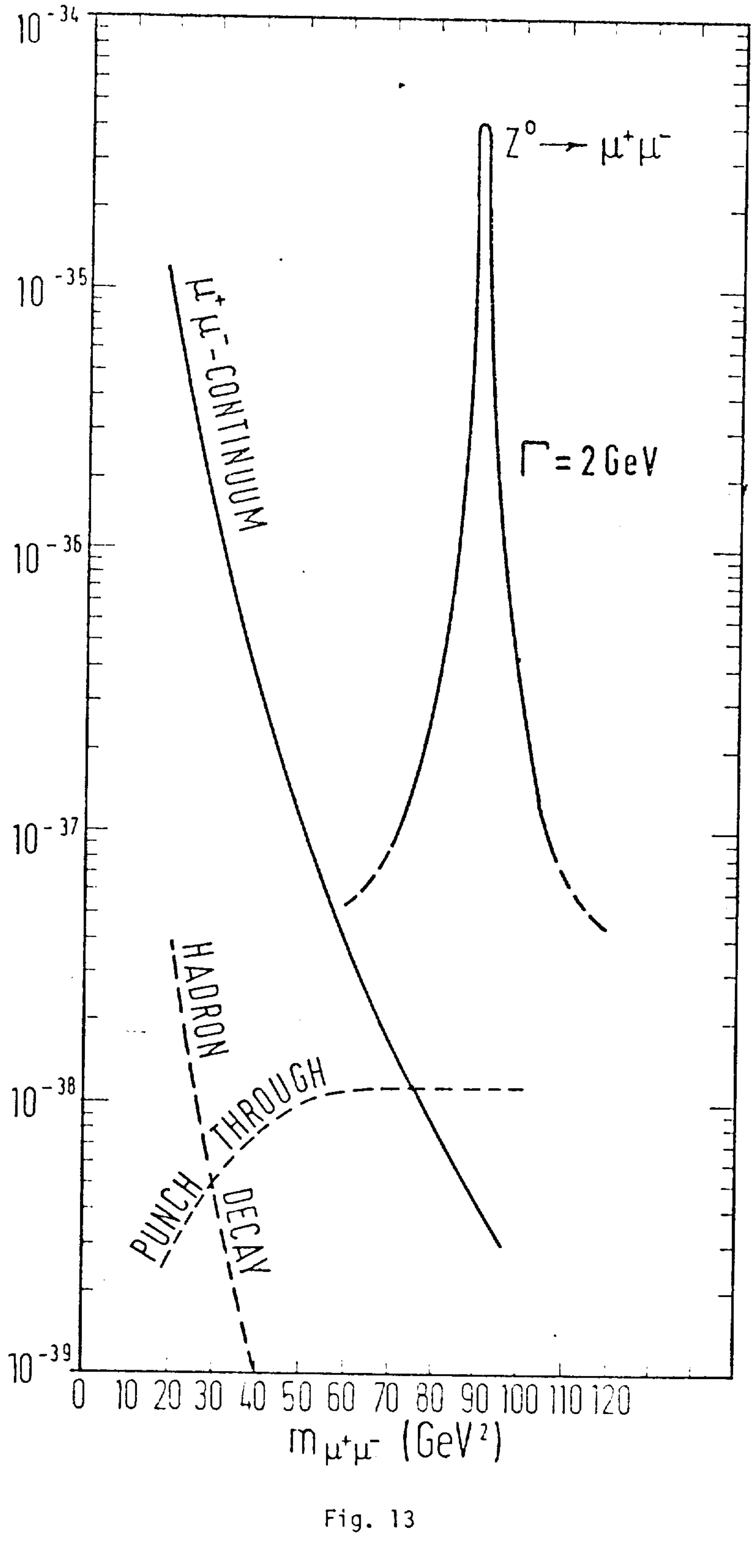

10^{-34}
10^{-35}
10^{-36}
10^{-37}
10^{-38}
10^{-39}
$Z^0 \rightarrow \mu^+\mu^-$
$\Gamma = 2$ GeV
$\mu^+\mu^-$-CONTINUUM
HADRON
PUNCH THROUGH
DECAY
0 10 20 30 40 50 60 70 80 90 100 110 120
$m_{\mu^+\mu^-}$ (GeV^2)

Fig. 13

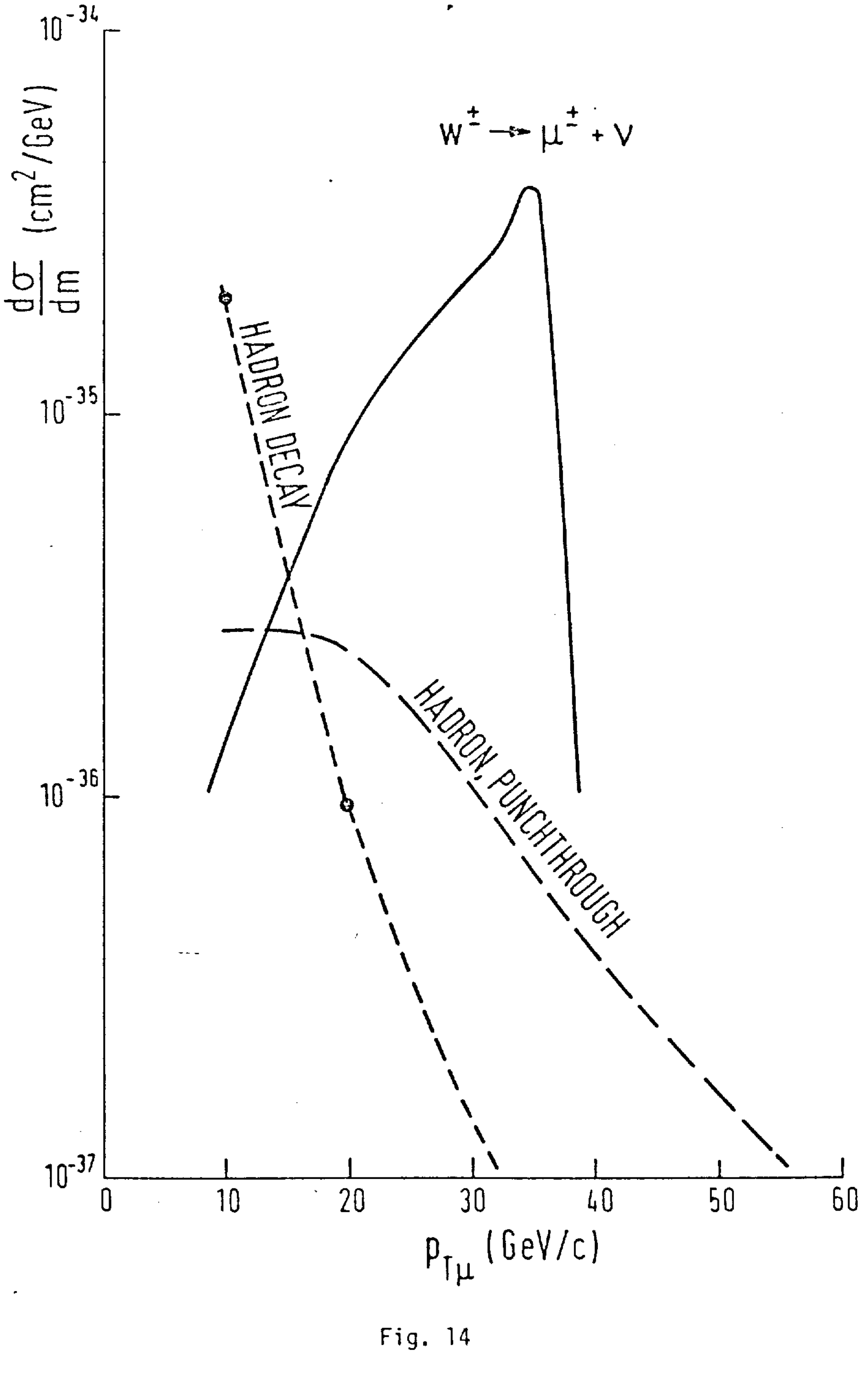

10^{-34}
10^{-35}
10^{-36}
10^{-37}
$\frac{d\sigma}{dm}$ (cm^2/GeV)
$W^{\pm} \rightarrow \mu^{\pm} + \nu$
HADRON DECAY
HADRON PUNCHTHROUGH
0
10
20
30
40
50
60
$p_{T\mu}$ (GeV/c)

Fig. 14

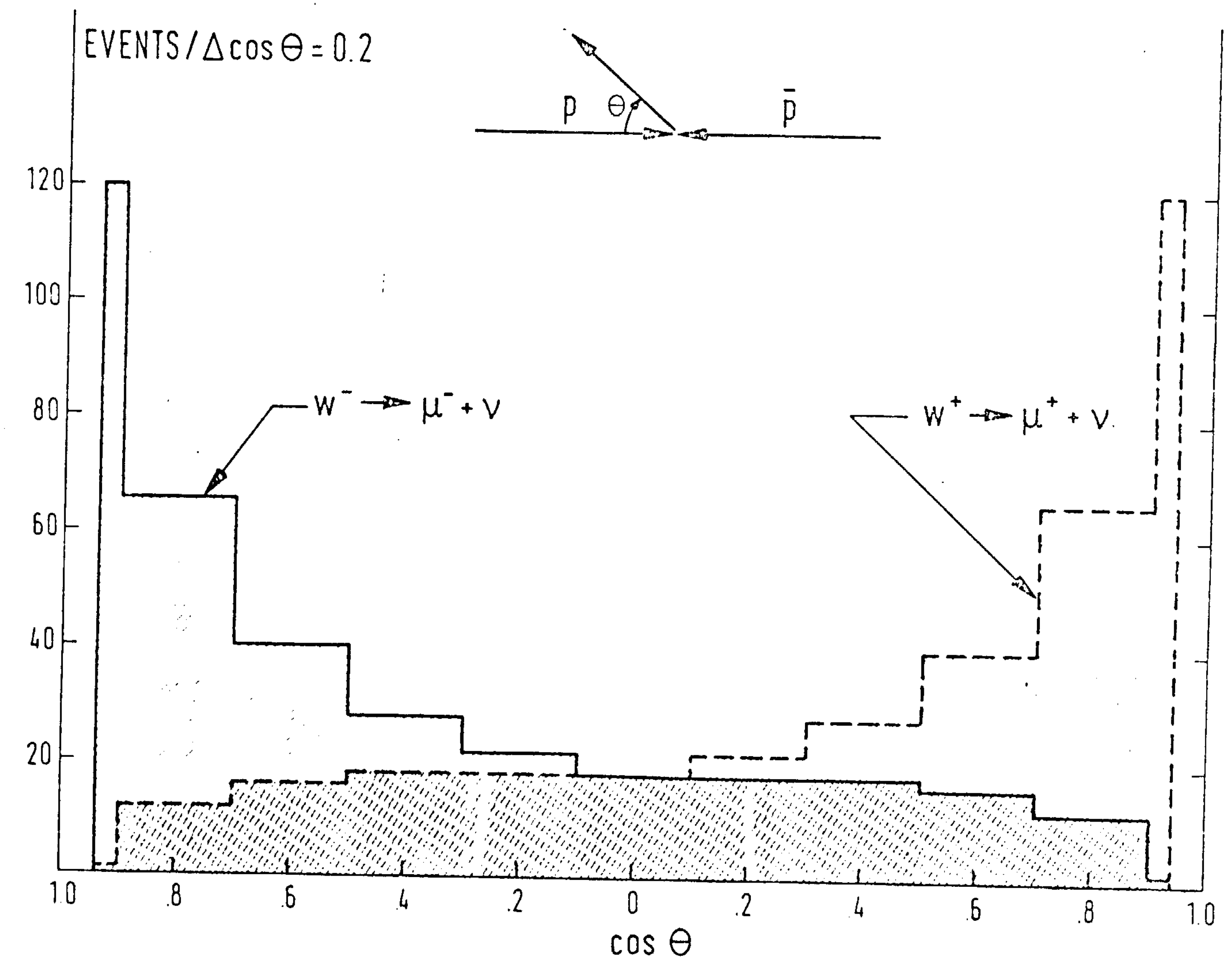
EVENTS/Δcos Θ = 0.2
p
Θ
p̄
120
100
80
60
40
20
W⁻ → μ⁻ + ν
W⁺ → μ⁺ + ν
1.0
.8
.6
.4
.2
0
.2
.4
.6
.8
1.0
cos Θ

Fig. 15